ADAPTIVE ESTIMATOR-CONTROLLER FOR SINGLE LINK FLEXIBLE MANIPULATOR

A DISSERTATION

Submitted in partial fulfillment of the
requirements for the award of the degree
of

MASTER OF TECHNOLOGY

in

ELECTRICAL ENGINEERING

(With specialization in Instrumentation and Signal Processing)

By

SHIKHA TOMAR

DEPARTMENT OF ELECTRICAL ENGINEERING
INDIAN INSTITUTE OF TECHNOLOGY ROORKEE
ROORKEE - 247 667 (INDIA)

MAY, 2016

CANDIDATE'S DECLARATION

I hereby declare that this thesis report entitled **ADAPTIVE ESTIMATOR-CONTROLLER FOR SINGLE LINK FLEXIBLE MANIPULATOR**, submitted to the Department of Electrical Engineering, Indian Institute of Technology, Roorkee, India, in partial fulfillment of the requirements for the award of the Degree of Master of Technology in Electrical Engineering with specialization in Instrumentation and Signal Processing is an authentic record of the work carried out by me during the period June 2015 through May 2016, under the supervision of **Dr. P. SUMATHI, Department of Electrical Engineering, Indian Institute of Technology, Roorkee.** The matter presented in this thesis report has not been submitted by me for the award of any other degree of this institute or any other institutes.

Date:

Place: Roorkee

Shikha Tomar

CERTIFICATE

This is to certify that the above statement made by the candidate is true to the best of my knowledge and belief.

Dr. P SUMATHI
Associate Professor
Department of Electrical Engineering
Indian Institute of Technology Roorkee

ABSTRACT

A vibration frequency estimator based on moving-window discrete Fourier transform (MWDFT) integrated with frequency locked loop (FLL) is proposed for the vibration mode estimation of single-link flexible manipulator (SLFM). A MWDFT exhibits tuned filter frequency response characteristics and this filter is considered as a digital system with negative feedback loop to track the tip deflection signal. The bandwidth of the MWDFT increases by the introduction of negative feedback. To estimate the frequency of the tip deflection signal, a FLL is designed with MWDFT-feedback loop. The frequency error was exploited to achieve synchronization between in-phase component of MWDFT and input signal. The existing frequency estimators and the FLL based on MWDFT are implemented on SLFM for the estimation of tip deflection signal amplitude and frequency.

An LQR controller is designed to control the tip deflection of SLFM which efficiently suppresses the tip deflection vibration.

Acknowledgements

I would like to express my deep sense of gratitude and sincere thanks to my guide **Dr. P. Sumathi**, Department of Electrical Engineering, Indian Institute of Technology Roorkee, for her valuable guidance and support. I am highly indebted to her for her encouragement and constructive criticism throughout the course of this project work. Inspite of her hectic schedule, she was always there for clarifying my doubts and reviewed my dissertation progress in a constructive manner. Without her help, this thesis would not have been possible.

Shikha Tomar

Contents

List of Figures

List of Tables

Abbreviations

FLL	**F**requency **L**ocked **L**oop
MWF	**M**oving **W**indow **F**ilter
DTI	**D**iscrete **T**ime **I**ntegrator
SPG	**S**ampling **P**ulse **G**enerator
MAF	**M**oving **A**verage **F**ilter
DFT	**D**iscrete **F**ourier **T**ransform
SOGI	**S**econd **O**rder **G**eneralised **I**ntegrator
DSP	**D**igital **S**ignal **P**rocessing
LQR	**L**inear **Q**uadratic **R**egulator

Chapter 1

Introduction

The flexible manipulators span a wide range of applications such as space robotics, collision control, nuclear maintenance and others. The problems related to flexible manipulators and their several applications can be found in the literature survey in [1]. The interest in the vibration frequency estimation of flexible manipulators is mainly due to the higher operating speeds, light weight, low energy consumption, safer operation due to reduced inertia, low mounting strength requirement, smaller actuator requirement, low rigidity, transportability and less bulky design. However, in realizing the advantages of flexible manipulator, vibration arising due to structural flexibility is a major constraint. There is an increased demand for high-speed robotics in industries resulting in the significant increase in the necessity of research on the control of flexible manipulators which includes vibration frequency estimations of the flexible link. Frequency estimation is the identification or extraction of nonstationary sinusoidal signals and the estimation of their parameters such as amplitude, frequency and phase. Examples of its general applications are frequency estimation of time-varying biomedical signals, active noise and vibration control, and sinusoidal disturbance rejection. The various methods proposed in the past for frequency estimation have been implemented on the flexible link manipulator and a technique for vibration frequency estimator is proposed.

1.1 Literature survey

Flexible-link manipulator control is achieved through Lyapunov control, fractional order controller, generalized proportional controller (GPI), intelligent control, integral resonant control (IRC), and adaptive control. In [2], dynamic deflection is measured using an optical sensing system comprising a laser diode and a position sensitive detector. A Lyapunov controller based on deflection feedback regulates the endpoint of the flexible manipulator and dampens it's oscillations. The tip position control in [3] is achieved with an output feedback control strategy based on the principle of transmission zero assignment; this ensures the stability of the closed-loop system. Further, the tip-position control is implemented with fractional order controller [4], where the overshoot of the system is independent of the tip mass. A motion controller using GPI is proposed in [5] to control the torque of SLFM for free and constrained motion. An intelligent-based control scheme in [6] motivated by inverse dynamics control strategy for rigid-link manipulators is proposed for the tip-position tracking control of flexible manipulator. The end-point vibration is dampened by the active vibration controller based on fuzzy logic and neural networks [7] [8]. Furthermore, an IRC scheme based technique consisting of two nested loops could be found in [9]. The output redefinition strategy and feedback linearization techniques are employed in [10]to adaptively control [11] [12] the manipulator.

The aforementioned control methods demand the output should be measured or estimated and fedback to the controller to take appropriate control action. A sensing strategy integrated with the filter design estimates the end point vibration rate of the single link flexible manipulator [13]. A control scheme based on strain guage is proposed for very lightweight single-link flexible manipulator in [14]. A vibration mode estimation method based on sliding discrete fourier transform integrated with phase-locked loop is proposed in [15]. An algebraic estimator is integrated with an adaptive controller to control the tip deflection of flexible manipulator [16]. Therefore, the capability of existing frequency estimators and their suitability to estimate the tip deflection frequency have been explored for integration of these methods with adaptive controllers.

The existing frequency estimators are (i) non-linear adaptive estimation (NLAE) [17], (ii) globally convergent (GC) [18], [19] (iii) algebraic identification (AI) [20],[21], (iv) second order generalized integrator (SOGI) based frequency locked loop [22], [23], [24], (v) third order generalized integrator (TOGI) based adaptive frequency locked loop (AFLL) [25].

The NLAE method for extraction of non-stationary sinusoids involves gradient descent method to minimize the error between input and desired signals. The convergence and stability of the system are guaranteed only if the error is quadratic. In addition, this method demands a nominal value of frequency ω_0 to be set close to the estimating frequency of the signal and when this nominal value deviates there exists a trade-off between the speed and steady-state error that results in an increased computation time. Another constraint is the choice of the parameters, which determines the convergence speed versus error compromise.

The GC method guarantees convergence and it reconstructs the values of frequency, amplitude, and offset of the signal simultaneously. The higher order estimator has smoother estimates than the lower order one due to the filtering of the transformed input signal. However, this method is not suitable for the signal, which is the addition of multiple sinusoidal signal of different amplitudes and frequencies. The AI estimator employs the time varying linear unstable filters along with classical low-pass filters. The estimator convergence is independent of the initial conditions and design parameter. However, the signal-to-noise ratio affects the performance exponentially.

The generalized integrator convolves the sinusoidal signal by itself in time-domain and yields the sinusoidal signal multiplied by time variable. The dynamic response of the SOGI based FLL depends on the amplitude and frequency of the input signal and control parameters. However, the SOGI based FLL should be modified for the estimation of multiple sinusoidal frequencies that are integer multiple of fundamental frequency. Moreover, structural modification is required for estimating the frequency of input sinusoidal signal with dc input. In TOGI based FLL, the dependence of dynamical response on the amplitude and frequency of input is reduced. This estimator is capable of estimating the unknown parameters in the presence of harmonic components in the input signal with order four. However, the small values of frequency result in slow-down of the dynamic response. Therefore, the previously proposed techniques aforementioned have one or more disadvantages as (i) convergence and stability is not guaranteed, (ii) there exists a compromise between the convergence speed and steady-state error, (iii) constraint in setting of parameters, (iv) not appropriate for multiple amplitude and multiple frequency estimation, (v) performance depends on SNR, (vi) dependency of stability and dynamic response on amplitude and frequency of the input signal and control parameters, and (vii) slow-down of the dynamic response at small values of frequency.

1.2 Objectives of dissertation work

The objectives of this dissertation work include:

1. Develop a dynamic model for the SLFM system.
2. Propose a frequency estimation scheme based on Moving-Window DFT.
3. Simulate the frequency estimator with different test inputs.
4. Implement the proposed scheme on SLFM system.
5. Evaluate the performance of the proposed scheme and compare it with the previously proposed estimation techniques.
6. Design an adaptive controller to suppress the oscillation of the link.

1.3 Organisation of report

This report is organized as follows: Chapter 2 describes the modeling of the SLFM. Overview of the frequency estimation techniques previously proposed is discussed in Chapter 3. The proposed technique alongwith the adaptive controller is presented in Chapter 4. Chapter 5 discusses the simulation and experimental results and performance comparison is done for all the techniques. Conclusions and scope for future work are stated in Chapter 6.

Chapter 2

Modeling of Single-Link Flexible Manipulator

2.1 Experimental set-up

The block diagram of the experimental set-up is shown in Fig. 3.4. The experimental setup under consideration is a single-link flexible manipulator which is coupled to a D.C. motor controlled rotary base. Quanser Flexible link system consists of (i) a rotary base (SRV02) and flexible link (ii) amplifier unit (iii) data acquisition (DAQ) system.

2.1.1 SRV02 servomotor

The SRV02 consists of a DC motor that is encased in a solid aluminium frame and provided with a gearbox. The motor drives external gears with the help of its own gearbox. SRV02 is equipped with potentiometer, encoder and tachometer. Optical encoder and potentiometer are used for measurement of angular position of motor shaft, tachometer is used to measure angular velocity of motor shaft.

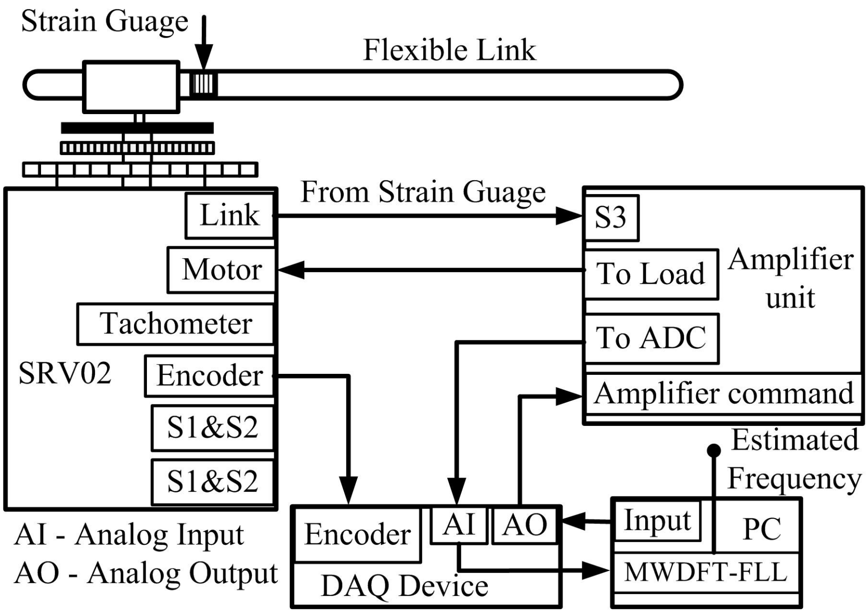

FIGURE 2.1: Block diagram representation of experimental set-up

2.1.2 Flexgage (Flexible link)

Flexgage is a single link exible manipulator whose base is mounted on the load gear of the SRV02 system. It has one degree of freedom and rotates in horizontal direction only. The main objective here is to suppress the vibrations at the tip of the link. The deflection of the tip is measured by the strain guage affixed at the motor end of exible link.

2.1.3 Voltage amplifier

The Quanser VoltPAQ-X1 is a single channel linear voltage based power amplifier. The main functions of voltage amplifier are to supply the required voltage and current to drive DC motor, provide power supply to all sensors of SRV02 and FLEXGAGE, receive outputs of all analog sensors and convert them to the required voltage levels to communicate with data acquisition device.

2.1.4 Data acquisition device

Quanser Q8-USB is a high performance data acquisition control board. DAQ device acquires data from sensors through voltage amplifier (for analog sensors only), converts it into digital format to communicate with PC as well as accept data in digital format from PC, and convert it to analog to give motor command. PC commands are communicated via USB port to DAQ device and fed to SLFM. QUARC control software integrated with MATLAB/simulink environment controls the input to SLFM.

2.2 Modeling of single link flexible manipulator

A dynamic model of system is required to be developed in order to know about the dynamics and the response of system with respect to different inputs. The equations that describe the motions of the servo and the link are obtained using the Euler-Lagrange equation.

$$\frac{\partial^2 L}{(\partial t \partial \dot{q_i})} - \frac{\partial L}{(\partial q_i)} = Q_i \tag{2.1}$$

where q_i are generalised coordinates, the two generalised coordinates are motor angular position $\theta(t)$ and tip deflection of link $x_\alpha(t)$.

$$q(t)^T = [\theta(t)x_\alpha(t)] \tag{2.2}$$

With the generalised coordinates defined, the Euler-Lagrange equation for the rotary flexible link system are

$$\frac{\partial^2 L}{\partial t \partial \dot{\theta}} - \frac{\partial L}{\partial \theta} = Q_1 \tag{2.3}$$

$$\frac{\partial^2 L}{\partial t \partial \dot{x_\alpha}} - \frac{\partial L}{\partial x_\alpha} = Q_2 \tag{2.4}$$

The generalised force acting on rotary arm is

$$Q_1 = \tau_l - B_{eq}\dot{\theta} \tag{2.5}$$

and the generalised force acting on flexible link is given as

$$Q_2 = -B_l \dot{x_\alpha} \tag{2.6}$$

Back emf voltage of motor is given by

$$e_b(t) = k_m \omega_m(t) \tag{2.7}$$

Differential equation obtained from DC motor armature circuit is

$$V_m - I_m R_m - L_m \frac{dI_m(t)}{dt} - k_m \omega_m(t) = 0 \tag{2.8}$$

where

$V_m(t)$ is input applied to SRV02

$\omega_m(t)$ is angular velocity of shaft measurement

$I_m(t)$ is armature current of motor.

Armature inductance L_m is very small, hence neglected in deriving the model. Armature current $I_m(t)$ is given by following equation

$$I_m(t) = \frac{V_m(t) - k_m \omega_m(t)}{R_m} \tag{2.9}$$

The motor torque $\tau_m(t)$ and the torque applied at load shaft $\tau_l(t)$ are

$$\tau_m(t) = \eta_m k_t I_m(t) \tag{2.10}$$

$$\tau_l(t) = \eta_g K_g \tau_m(t) \tag{2.11}$$

Using equation (2.9) (2.10) and (2.11), $\tau_l(t)$ is given as

$$\tau_l(t) = \frac{\eta_g K_g \eta_m k_t (V_m - K_g k_m \dot{\theta})}{R_m} \tag{2.12}$$

The Lagrangian operator is

$$L = K - P$$

where K is kinetic energy and P is potential energy.

Therefore,

$$L = \frac{1}{2} J_{eq} \dot{\theta}^2 + \frac{1}{2} J_l (\dot{\theta} + \dot{x_\alpha})^2 - \frac{1}{2} K_s x_{\alpha^2} \tag{2.13}$$

where J_{eq} is moment of inertia and B_{eq} is viscous friction.

This friction opposes the torque being applied at the servo load gear. The friction acting on the link is represented by viscous damping coefficient B_l. Flexible link can be modeled as a linear spring with stiffness K_s. The state variables chosen for the model are $\theta, x_\alpha, \dot{\theta}$ and $\dot{x_\alpha}$.

$$(J_{eq} + J_l)\ddot{\theta} + J_l \ddot{x_\alpha} + B_{eq} \dot{\theta} = \tau_l \tag{2.14}$$

$$J_l \ddot{\theta} + J_l \ddot{x_\alpha} + B_l \dot{\theta} + K_s x_\alpha = 0 \tag{2.15}$$

TABLE 2.1: Parameter values of experimental set-up

Parameters	Symbol	Unit	Value
Motor armature resistance	R_m	ω	2.6
Motor armature inductance	L_m	H	$0.18x10^{-3}$
Motor back emf constant	k_m	$V/(rad/s)$	$7.68x10^{-3}$
Motor torque constant	k_t	$N.m/A$	$7.68x10^{-3}$
Viscous friction acting on motor shaft	B_m	$N.m/(rad/s)$	0.015
Motor shaft moment of inertia	J_m	$kg.m^2$	$9.76x10^{-5}$
Motor efficiency	η_m		0.69
Gearbox efficiency	η_g		0.9
Gear ratio	K_g		70
Length of link	L	m	0.419
Mass of link	M	kg	0.065
Viscous friction acting on link	B_l	$N.m/(rad/s)$	0
Link moment of inertia	J_l	$kg.m^2$	0.0038
Link stiffness coefficient	K_s	$N.m/rad$	1.3

Using equations (2.14) and (2.15), Euler-Lagrange equations are

$$\ddot{\theta} = -(\frac{B_{eq}}{J_{eq}} + \frac{\eta_g K_g^2 k_m k_t \eta_m}{J_{eq} R_m})\dot{\theta} + \frac{K_s}{J_{eq}} x_\alpha + \frac{\eta_g K_g \eta_m k_t}{J_{eq} R_m} V_m \tag{2.16}$$

$$\ddot{x_\alpha} = (\frac{B_{eq}}{J_{eq}} + \frac{\eta_g K_g^2 k_m k_t \eta_m}{J_{eq} R_m})\dot{\theta} - K_s(\frac{J_l + J_{eq}}{J_l J_{eq}}) x_\alpha - \frac{\eta_g K_g \eta_m k_t}{J_{eq} R_m} V_m \tag{2.17}$$

where

$J_{eq} = \eta_g K_g^2 J_m + J_l$

$B_{eq} = \eta_g K_g^2 B_m + B_l$

State space representation of single link flexible manipulator is

$$\dot{x} = Ax + Bu \tag{2.18}$$

$$y = Cx + Du \tag{2.19}$$

where,

$$A = \begin{bmatrix} 0 & 0 & 1 & 0 \\ 0 & 0 & 0 & 1 \\ 0 & \frac{K_s}{J_{eq}} & -(\frac{B_{eq}}{J_{eq}} + \frac{\eta_g K_g^2 k_m k_t \eta_m}{J_{eq} R_m}) & 0 \\ 0 & -K_s(\frac{1}{J_{eq}} + \frac{1}{J_l}) & (\frac{B_{eq}}{J_{eq}} + \frac{\eta_g K_g^2 k_m k_t \eta_m}{J_{eq} R_m}) & 0 \end{bmatrix}$$

$$B = \begin{bmatrix} 0 \\ 0 \\ \frac{\eta_g K_g \eta_m k_t}{J_{eq} R_m} \\ -\frac{\eta_g K_g \eta_m k_t}{J_{eq} R_m} \end{bmatrix}; C = \begin{bmatrix} 1 & 0 & 0 & 0 \\ 0 & 1 & 0 & 0 \\ 0 & 0 & 1 & 0 \\ 0 & 0 & 0 & 1 \end{bmatrix}; D = \begin{bmatrix} 0 \\ 0 \\ 0 \\ 0 \end{bmatrix}$$

Chapter 3

Frequency Estimators overview

3.0.1 Non-linear adaptive method

The dynamics of the algorithm for the extraction of nonstationary exponentially decaying sinusoidal signal and estimation of their parameters is governed by a set of non linear differential equations as given below [17].

$$y(t) = A \sin \phi(t);\ \phi(t) = \omega t + \theta$$

$$\begin{aligned}
\frac{d\hat{A}(t)}{dt} &= 2\mu_1 e(t) \sin \hat{\phi}(t) \\
\frac{d\hat{\omega}(t)}{dt} &= 2\mu_2 e(t) \hat{A}(t) \cos \hat{\phi}(t) \\
\frac{d\hat{\phi}(t)}{dt} &= \hat{\omega}(t) + \mu_3 \frac{d\hat{\omega}(t)}{dt} \\
e(t) &= u(t) - \hat{A}(t) \sin \hat{\phi}(t)
\end{aligned} \tag{3.1}$$

where, μ_1, μ_2, μ_3 are the algorithm regulating constants. This method requires a nominal value of frequency ω_0 to be set close to the frequency of the signal. As this nominal value deviates, there exists a trade-off between the speed and steady-state error. Another constraint is the setting of the parameters μ_1, μ_2, μ_3 which determine the convergence speed versus error compromise.

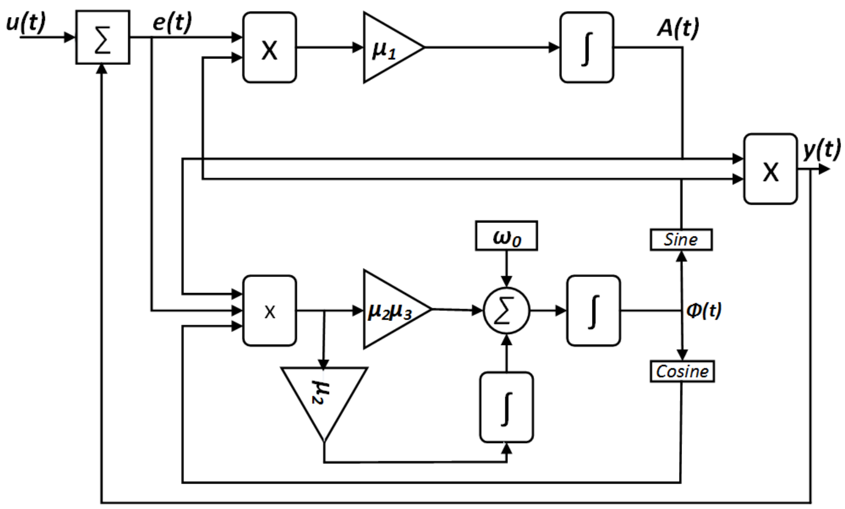

FIGURE 3.1: Block diagram for Nonlinear adaptive estimator

3.0.2 Globally convergent method

A method of estimation with the global convergence property to reconstruct the unknown values of the amplitude, frequency and offset of a sinusoidal signal simultaneously. A globally convergent estimator can be derived by defining a state variable as the time derivative of a quadratic function of the sinusoidal signal and using a technique in reduced-observer designs. Only frequency estimation possible in second order estimator, the reconstruction of other unknown values leads to the higher order estimators with smoother estimates [18].

$$y(t) = A_0 + A\sin(\omega t + \phi)$$

The derived seventh order estimator is as

$$\begin{aligned}
\dot{\xi}_1 &= -\lambda\xi_1 + 3\lambda y(t) \\
\dot{\xi}_2 &= -\lambda\xi_2 - 2\lambda y^2(t) \\
\dot{\hat{z}}_1 &= \hat{z}_2 + \xi'\hat{\theta} + (1+\alpha\lambda)(\lambda y^2(t)/2 - \hat{z}_1) \\
\dot{\hat{z}}_2 &= \lambda\xi'\hat{\theta} + \alpha(\lambda y^2(t)/2 - \hat{z}_1) \\
\dot{\hat{\theta}} &= \Gamma\xi(\lambda y^2(t)/2 - \hat{z}_1) \\
\theta &= [\theta_0\ \theta_1\ \theta_2] \\
\theta_0 &= (A^2 - A_0^2)\omega^2 \\
\theta_1 &= A_0\omega^2 \\
\theta_2 &= \omega^2
\end{aligned} \tag{3.2}$$

This estimator cannot be extended to the case of multiple amplitudes and frequencies. The convergence time is high for this estimator as revealed by the simulations.

3.0.3 Algebraic identification method

The problem of on line identification of unknown parameters, namely, amplitude, frequency and phase in unknown noisy sinusoidal signals is explored by an algebraic approach. An algebraic derivative method is employed in frequency domain which yields exact formulae for the unknown parameters when placed in time domain. The Butterworth type low-pass filters are applied to the time-varying linear unstable filters which result from the algeabraic manipulations performed on the Laplace transform expression of the biased signal to synthesize these formulae. The algeabraic manipulations above involve elimination of the unknown constants through derivation with respect to the complex frequency variable s [20].

$$y(t) = A_0 + A\sin(\omega t + \phi)$$
$$\gamma = [\gamma_1\ \gamma_2\ \gamma_3];\ \gamma_1 = \omega^2;\ \gamma_2 = A\sin\phi;\ \gamma_3 = A\omega\cos\phi;$$

The numerator and denominator signals are filtered using same low-pass filter. This does not affect the quotient. The low-pass filter is a second order filter with cut-off frequency ω_n and enhanced damping features.

$$\hat{\gamma_1} = \frac{n_1 F(s)}{d_1 F(s)}$$
$$F(s) = \frac{\omega_n^2}{s^2 + 2\zeta\omega_n s + \omega_n^2}$$

The numerator and denominator are obtained by differentiating the y(t) three times with respect to complex frequency s and are given as

$$\begin{aligned} n_1(t) &= z_1 + t^3 y(t), d_1(t) = z_4, \\ \dot{z_1} &= z_2 - 9t^2 y(t), \dot{z_2} = z_3 + 18ty(t), \\ \dot{z_3} &= -6y(t), \dot{z_4} = z_5, \\ \dot{z_5} &= z_6 - t^3 y(t), \dot{z_6} = 3t^2 y(t) \end{aligned} \tag{3.3}$$

The parameter γ_2 is obtained as follows and second order low-pass filter is applied to both numerator and denominator.

$$\begin{aligned}\hat{\gamma_2} &= \frac{n_2 F(s)}{d_2 F(s)}\\ n_2(t) &= \gamma_{21} + 2\hat{\gamma_1}\gamma_{22} + \hat{\gamma_1}^2\gamma_{23} - \hat{\gamma_1}\hat{\gamma_3}\frac{t^4}{24} + \hat{\gamma_3}\frac{t^2}{2},\end{aligned} \tag{3.4}$$

$$\begin{aligned}d_2(t) = -\frac{t^3\hat{\gamma_1}}{3}, \gamma_{21} = z_1 - ty(t),\\ \dot{z}_1 = y(t), \gamma_{22} = z_2,\\ \dot{z}_2 = z_3, \dot{z}_3 = z_4 - ty(t),\\ \dot{z}_4 = y(t), \gamma_{23} = z_5,\\ \dot{z}_5 = z_6, \dot{z}_6 = z_7,\\ \dot{z}_7 = z_8, \dot{z}_8 = z_9 - ty(t),\\ \dot{z}_9 = y(t)\end{aligned} \tag{3.5}$$

For the estimation of parameter γ_3, multiply the Laplace transform of y(t) by s and differentiate with respect to s and then multiplying the obtained expression by $(s^2 + p_1^2)^2$ and simplifying results into an expression which is further differentiated twice with respect to s, the equations obtained are as follows

$$\begin{aligned}\hat{\gamma_3} = \frac{n_3 F(s)}{d_3 F(s)}\\ n_3(t) = \gamma_{31} + \hat{\gamma_1}\gamma_3 2 + \hat{\gamma_1}^2\gamma_{33},\\ d_3(t) = \frac{-t^4}{12}, \gamma_{31} = z_1 - t^3 y(t),\end{aligned}$$

$$\begin{aligned}
\dot{z}_1 = z_2 + 11t^2y(t), \dot{z}_2 = z_3 - 28ty(t), \\
\dot{z}_3 = 12y(t), \gamma_{32} = z_4, \\
\dot{z}_4 = z_5, \dot{z}_5 = z_6 - 2t^3y(t), \\
\dot{z}_6 = z_7 + 14t^2y(t), \dot{z}_7 = z_8 - 20ty(t), \\
\dot{z}_8 = 4y(t), \gamma_{33} = z_9, \\
\dot{z}_9 = z_{10}, \dot{z}_{10} = z_{11}, \\
\dot{z}_{11} = z_{12}, \dot{z}_{12} = z_{13} - t^3y(t), \\
\dot{z}_{13} = 3t^2y(t)
\end{aligned} \tag{3.6}$$

The estimation of the frequency by this method is not smooth, it involves irregularities.

3.0.4 Second order generalized integrator based frequency locked loop

A second order generalised integrator (SOGI) together with the frequency locked loop (FLL) makes an adaptive system for the estimation of frequency and amplitude. The concept of the integrator comes from the principle that the original function multiplied by the time variable is obtained from the time-domain convolution product of a sinusoidal function by itself. A resonator is a processing block whose transfer function matches with the Laplace transform of a sinusoidal signal acts as an amplitude integrator for the signal applied at its input. An ideal integrator independent of the phase angle of the sinusoidal input signal can be obtained by the in-quadrature combination of the sine and cosine transfer functions. The frequency locked loop (FLL) here is an effective mechanism for adapting the center frequency of the SOGI based FLL. FLL detects the input frequncy directly and phase angle and amplitude are calculated indirectly. The dynamical response and stability of this nonlinear system depends on various parameters: the values of K and γ which are the control parameters of SOGI and FLL respectively and the frequency and amplitude of the signal [23] .

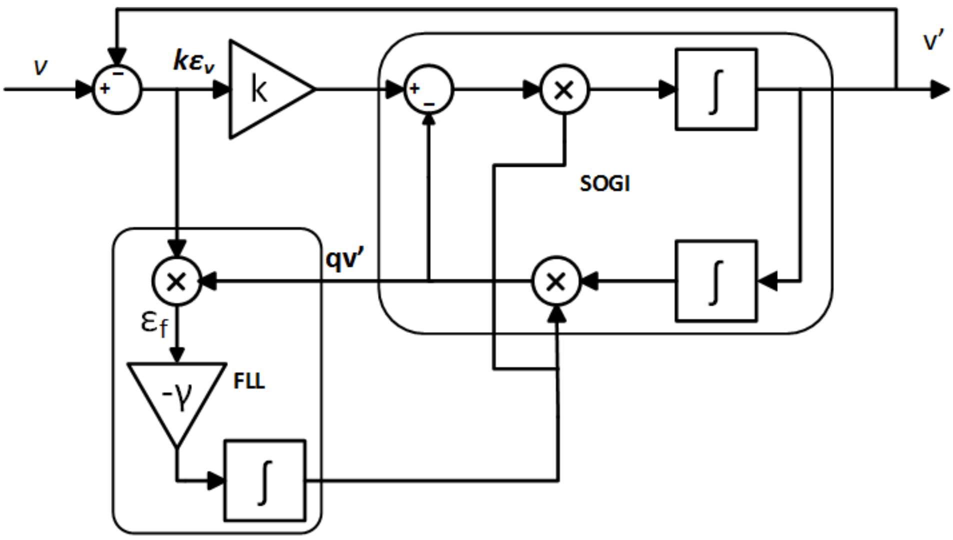

FIGURE 3.2: Adaptive filter based on SOGI

$$y(t) = A\sin(\omega t + \phi)$$

$$\begin{bmatrix} \dot{x}_1 \\ \dot{x}_2 \end{bmatrix} = \begin{bmatrix} -k\omega' & -\omega'^2 \\ 1 & 0 \end{bmatrix} \begin{bmatrix} x_1 \\ x_2 \end{bmatrix} + \begin{bmatrix} k\omega' \\ 0 \end{bmatrix} y \tag{3.7}$$

$$\begin{bmatrix} v' \\ qv' \end{bmatrix} = \begin{bmatrix} 1 & 0 \\ 0 & \omega' \end{bmatrix} \begin{bmatrix} x_1 \\ x_2 \end{bmatrix} \tag{3.8}$$

$$\dot{\omega}' = -\gamma x_2 \omega'(y - x_1) \tag{3.9}$$

3.0.5 Third order generalized integrator

A continuous-time on-line adapted frequency locked-loop (AFLL) filter based on a third order generalised integrator estimates the unknown parameters of a single baised sinusoidal signal with a dynamic of order four. The AFLL system is a third order filter described by the following differential system [25]

$$y(t) = A_0 + A\sin\theta(t),\, \theta(t) = \omega t + \phi$$

$$\begin{aligned} \dot{y}_1(t) &= -\omega' y_2(t) + K\omega'(Ky(t) - y_1(t)) \\ \dot{y}_2(t) &= \omega' y_1(t) \\ \dot{y}_3(t) &= -K\omega' y_3(t) + K\omega'(Ky(t) - y_1(t)) \end{aligned} \tag{3.10}$$

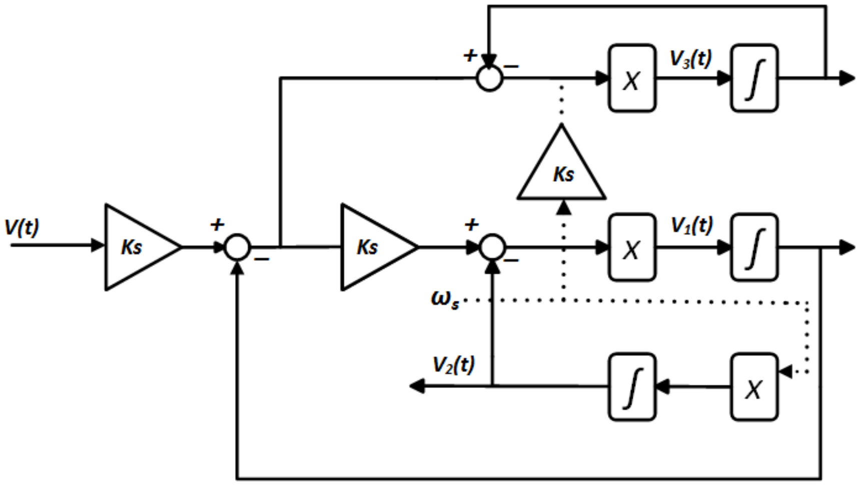

FIGURE 3.3: AFLL block diagram

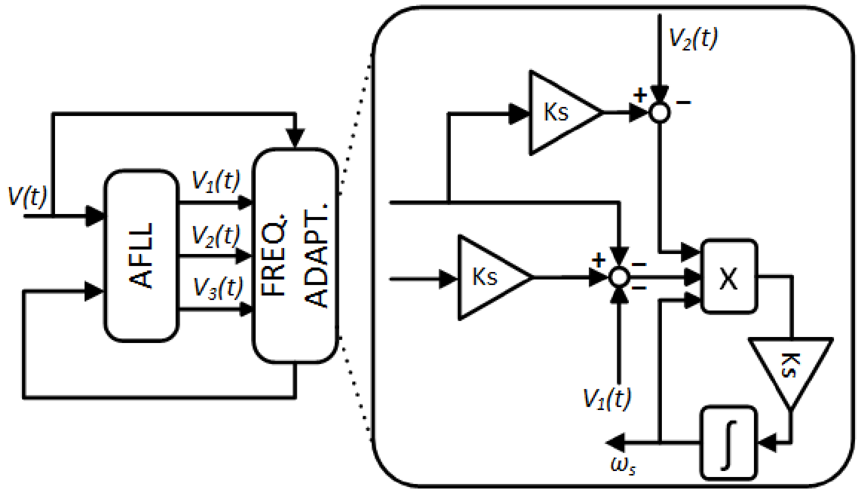

FIGURE 3.4: AFLL frequency adaptation scheme

where ω' and K represent the AFLL resonant frequency and the filter gain respectively. These two parameters define the dynamic and filtering characteristics completely. K affects the bandwidth of the system and $K\omega'$ adjusts the transient period. The adaptation law for ω' to tune the resonant frequency to the unknown is

$$\dot{\omega}'(t) = \gamma\omega'(t)(Ky(t) - y_1(t) - y_3(t))(Ky_3(t) - y(_2(t)); \gamma > 0 \tag{3.11}$$

The dynamic response is slower for small values of frequency.

Chapter 4

Proposed Scheme

4.1 MWDFT algorithm integrated with FLL

A moving window discrete Fourier transform (MWDFT) algorithm integrated with frequency locked loop (FLL) shown in 4.1 is proposed for vibration frequency estimation of single link flexible manipulator. This estimation scheme consists of (i) MWDFT with feedback and (ii) sampling pulse generator (SPG) for MWDFT.

4.1.1 MWDFT with feedback-loop

The basic idea behind the existence of moving window discrete fourier transform is derived from the fact that there are more number of identical elements at two consecutive time instants. Consider the two time instances as $(n1)$ and n with corresponding sequences as $y(n1)$ and $y(n)$. For window length of $N = 32$, and for time instant $n = 31$ sequence is as follows [26]

$$y(31) = y(0), y(1), ...y(31)$$

and $y(32)$ is given as at time instant n=32

$$y(32) = y(1), y(2), ...y(32)$$

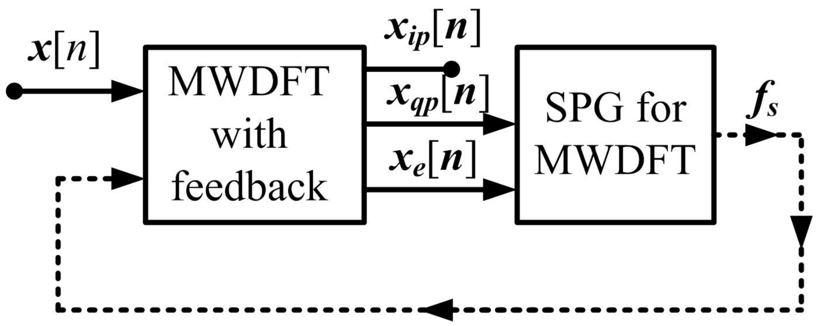

FIGURE 4.1: Block diagram of proposed frequency-locked loop

The moving window DFT algorithm performs an N-point DFT on time samples within a sliding window. For the above example, the MWDFT initially computes the DFT of the N=32 samples and then the time window is advanced one sample and a new N-point DFT is calculated. The incremental advance of time window leads to the name moving window DFT. DFT of current time instant is calculated using DFT of previous instant with minimum number of computations.

From properties of DFT,

If $Y[k]$ be N-DFT corresponding to $y[n]$, then

$$y[(n-m)N] = W_N^{km} Y[k] \tag{4.1}$$

where

$$W_N = e^{-j2\pi/N} \tag{4.2}$$

where N is the window length.

The property in (4.1) is circular shift property of DFT. First sequence element is replaced by the last sequence element, for e.g. y(0) is replaced by y(32) in y(31) and circularly shift the sequence obtained to the left by one sample.

Therefore, the result of the above is

$$Y_k(n) = [Y_k(n-1) - y(n-N) + y(n)]e^{j2\pi k/N} \tag{4.3}$$

Using this formula, transfer function of MWDFT in z-domain is as follows

$$H(z) = \frac{(1-z^N)e^{j2\pi k/N}}{1-e^{j2\pi k/N}z^{-1}} \tag{4.4}$$

MWDFT is more efficient compared to the convention DFT and FFT algorithms. It requires fixed number computations, that is, two real additions and one complex multiplication irrespective of the length of DFT. However, for this algorithmic computation, it is essential that DFT for previous time instant is available. A

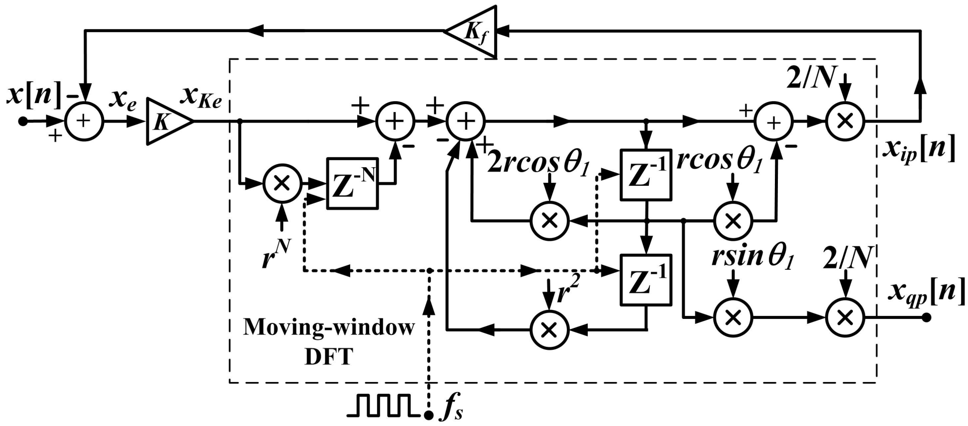

FIGURE 4.2: MWDFT feedback-loop

simple idea to initialize this algorithm is to obtain DFT of first time instant either using DFT or FFT [27].

The block diagram of MWDFT in feedback-loop is shown in Fig. 4.2.

The MWDFT computes the N-point DFT of the tip deflection signal $x[n]$ by advancing the window of width N with one sample [26], [27], [28]. The difference equation of MWDFT is

$$X_k(n) = [X_k(n-1) - x(n-N)r^N + x(n)]re^{j\theta_k} \tag{4.5}$$

where, k is the bin index; $\theta_k = 2\pi k/N$; r is the damping factor; $X_k(n)$ is the DFT at present instant; and $X_k(n-1)$ is the DFT at previous instant. For $k = 1$, the transfer function obtained in z-domain with multiplying factor $(2/N)$ is

$$H_{MWDFT}(z) = \frac{2}{N}\frac{(1-r^N z^N)re^{j\theta_1}}{1-re^{j\theta_1}z^{-1}} \tag{4.6}$$

The input to MWDFT is $x_{Ke}[n]$, the difference between $x[n]$ and in-phase component $x_{ip}[n]$ obtained at the output. Let the tip deflection be

$$x[n] \;=\; Ae^{-\zeta n}\sin(\omega n) \tag{4.7}$$

where A and ω are the amplitude and angular frequency of tip deflection to be estimated; ζ is decaying ratio. For fixed sampling frequency f_s, the tip deflection

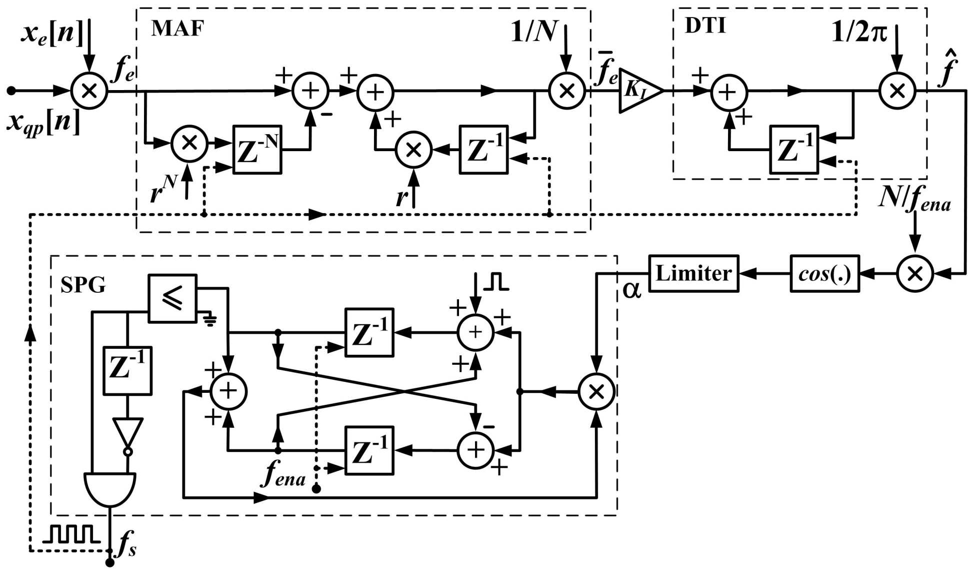

FIGURE 4.3: Schematic of sampling pulse adjustment mechanism

frequency (ω) variation can be modeled in the MWDFT output x_{ip} and x_{qp} as

$$
\begin{aligned}
x_{ip} &= A_1 e^{-\zeta n} sin(\omega n \pm \phi) \\
x_{qp} &= A_2 e^{-\zeta n} cos(\omega n \pm \phi)
\end{aligned}
\tag{4.8}
$$

where A_1 and A_2 are the amplitudes of x_{ip} and x_{qp}. The ϕ is phase shift observed at x_{ip} and x_{qp} due to the change in ω. The change in center frequency of ω introduces changes in amplitude (increase or decrease) and phase shift (lead or lag), i.e. windowing effect of DFT in x_{ip} and x_{qp}. The bandwidth of MWDFT tuned digital filter is increased through negative feedback and the frequency response is made almost flat characteristics. However, the sampling frequency mechanism is integrated with the FLL to eliminate the small magnitude and phase error observed at x_{ip} and x_{qp}. Therefore, the error

$$
x_e[n] = x[n] - K_f x_{ip}[n] \tag{4.9}
$$

4.1.2 SPG for MWDFT

The block diagram representation of adaptive sampling pulse adjustment scheme is shown in Fig.4.3. It consists of moving average filter (MAF), discrete-time integrator (DTI) [29] and sampling pulse generator (SPG).

For $K_f = 1$,

$$\begin{aligned} x_e[n] &= e^{-\zeta n}[Asin(\omega n) - A_1 sin(\omega n \pm \phi)] \\ x_e[n] &= e^{-\zeta n} Rsin(\omega n - \theta) \end{aligned} \tag{4.10}$$

where $R = \sqrt{a^2 + b^2}$; $a = [A - A_1 cos(\phi)]$; $b = A_1 sin(\phi)$; $\theta = \arctan(b/a)$. The input to the sampling pulse adjustment mechanism is the $x_e[n]$ multiplied with x_{qp} of MWDFT as shown in Fig.4.3. The frequency error is

$$f_e[n] = \frac{A_2 e^{-2\zeta n} R}{2}[sin(2\omega n + \theta \pm \phi) - sin(\theta \pm \phi)] \tag{4.11}$$

The $f_e[n]$ is fed to MAF.

4.1.2.1 Moving average filter

Moving average lter acts as low pass lter and passes on average value and blocks fundamental and harmonics. In Z-domain the transfer function is given as

$$H_{MA}(z) = \frac{1}{N}\frac{1 - z^{-N}}{1 - z^{-1}} \tag{4.12}$$

Number of computations required for above mentioned filter are 1 addition, 1 subtraction along with constant multiplication for each output sample irrespective of window length that is N.

4.1.2.2 PI controller

The purpose behind the PI controller is to produce constant DC input to NCO at steady state that is when output of phase detector i.e. e(n) approaches zero. In Z-domain PI controller is designed using following equation

$$H_{PI}(z) = K_p + \frac{K_i}{1 - z^{-1}} \tag{4.13}$$

4.1.2.3 Limiter

Limiter is used to limit the saturation level of integral action of PI controller, which indirectly bounds the value of control input supplied to NCO. Therefore control input to NCO is limited in between -1 and 1.

4.1.2.4 Numerically controlled oscillator

Numerically controlled oscillator receives the control input in range of -1 to 1 to generate the pulses of required frequency which are further fed to the MWDFT and moving average filter [29].
Let α is the control input to NCO
where,

$$\alpha = cos\omega t \tag{4.14}$$

$$\alpha = cos(\frac{2\pi f_s}{f_{enable}}) \tag{4.15}$$

for $\alpha = 0$, $f_{enable} = 4f_s$, where, f_{enable} is the enabling frequency and this technique works at 4 times the sampling frequency.
NCO is implemented using the following equation

$$\begin{bmatrix} y_1(k+1) \\ y_2(k+1) \end{bmatrix} = \begin{bmatrix} \alpha & \alpha - 1 \\ \alpha + 1 & \alpha' \end{bmatrix} \begin{bmatrix} y_1(k) \\ y_2(k) \end{bmatrix} \tag{4.16}$$

initial conditions are $y_1(0) = 1$ and $y_2(0) = 0$.

4.1.3 Proposed method

The signal form the deflection of the tip x_α is measured by the strain guage which is fed to the input of the MWDFT. The in-phase x_{ip} and quadrature-phase x_{qp} components are obtained in z-domain at the output of MWDFT from (4.6) as

$$\begin{aligned} Re[H_{MWDFT}(z)] &= \frac{2}{N}\frac{(1 - r^N z^{-N})(r\cos\theta_1 - r^2 z^{-1})}{1 - 2r\cos\theta_1 z^{-1} + r^2 z^{-2}} \\ Im[H_{MWDFT}(z)] &= \frac{2}{N}\frac{(1 - r^N z^{-N})(r\sin\theta_1)}{1 - 2r\cos\theta_1 z^{-1} + r^2 z^{-2}} \end{aligned} \tag{4.17}$$

where, N is the window length and r is the damping factor.
The comb filter cascaded with resonator structure of (4.17) is shown in Fig. 4.2. This filter is marginally stable because of the pole lying on the unit circle in z-domain. The damping factor ensures the stability of the MWDFT as it forces the pole to be at a radius of $r < 1$ (inside the unit circle). MWDFT extracts the fundamental of tip deflection signal $x[n]$ to estimate it's amplitude and frequency.

This method is designed to extract the fundamental signal of tip deflection from ideally 0 Hz to 6 Hz with center frequency of 3 Hz. The product of error and output of the MWDFT algorithm is fed to the moving averager which smoothens the error by eliminating the high frequencies. This avarage error is further processed by the proportional integral controller and the resultant signal is limited by the saturation block. This signal is then supplied to the numerically controlled oscillator (NCO) whose output adjusts the sampling frequency of MWDFT whenever the tip deflection varies around the input frequency. The NCO supplies the correct sampling frequency required for the MWDFT and moving averager.

4.2 Controller

The control for SLFM is obtained using Linear Quadratic Regulator (LQR). If the matrices A and B are controllable, then the Linear Quadratic Regulator optimization method is used to find a feedback control gain. The model is given in (2.18), the control input u is found that minimizes the cost function

$$J = \int_0^\infty x(t)'Qx(t) + u(t)'Ru(t)dt \tag{4.18}$$

where Q and R are the weighting matrices. These matrices are essentially the tuning variables which affect how LQR minimizes the cost function.

The control law is given as $u = -Kx$, the state-space equation in (2.18) becomes

$$\dot{x} = Ax + B(-Kx)$$
$$\dot{x} = (A - BK)x$$

The feedback control loop is designed which stabilizes the servo to a desired position θ_d, while minimizing the deflection of the flexible link.
The reference state is defined as

$$x_d = [\ \theta_d\ 0\ 0\ 0\ ]$$

and the controller as

$$u = K(x_s - x)$$

If x_d is 0, then $u = -Kx$, which is same as the control used in the LQR algorithm. The Q and R matrices are tuned, and the gain K is generated using LQR which minimizes the function.

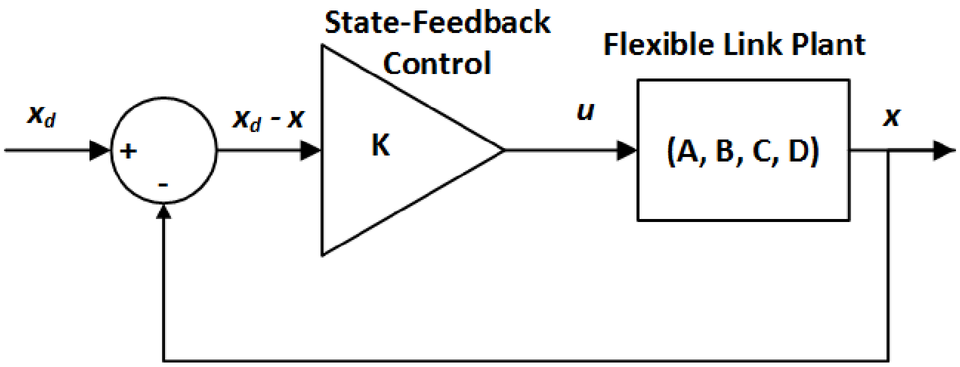

FIGURE 4.4: State-feedback Control Loop

In full state feedback, both the servo position and the flexible link position along with their velocity states are fedback. In partial state feedback (PSF), the strain guage is ignored and only the servo position control is achieved.

$$Q = \begin{bmatrix} q_1 & 0 & 0 & 0 \\ 0 & q_2 & 0 & 0 \\ 0 & 0 & q_3 & 0 \\ 0 & 0 & 0 & q_4 \end{bmatrix};\ R = 1$$

The matrix Q sets the weight on the states which determines u to minimize J. Also, increasing or decreasing the diagonal elements of Q, effects the generated gain $K = [k_1\ k_2\ k_3\ k_4]$.

The increase in q_1 increases the servo proportional gain k_1 which makes the system response faster by decreasing peak and settling time. q_2 does not affect the system response. An increase in q_3 increases the servo derivative gain k_3 and makes

k_4 more positive thereby minimizing the overshoot of servo response. This has a disadvantage of slowing down the response. On increasing q_4, the link proportional gain k_2 and derivative gain k_4 decreases. This significantly minimizes the deflection of flexible link without affecting the servo related gains, k_1 and k_3.

Chapter 5

Results and Discussions

The performance of the proposed algorithm is presented in this section. The proposed scheme is implemented for the frequency estimation of single-link flexible manipulator. The simulation and experimental results are discussed. Performance of proposed algorithm is compared with following frequency estimation techniques.

1. Non-linear adaptive method
2. Globally convergent method
3. Algebraic identification method
4. Second order generalised integrator based frequency-locked loop
5. Third order generalised integrator

5.1 Simulation results

The aforementioned frequency estimation methods are simulated with the synthetic vibration signal generated in the MATLAB/Simulink environment.

5.1.1 Frequency and amplitude estimation

In non-linear adaptive estimator, the parameters are chosen as $\mu_1 = 50$ $\mu_2 = 0.25$ and $\mu_3 = 2000$.

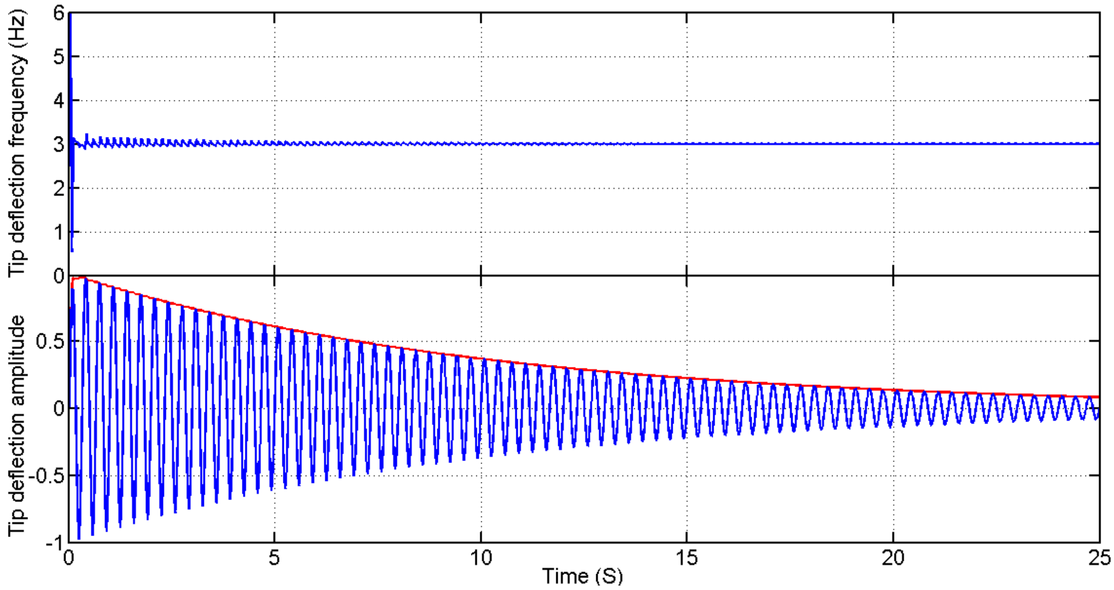

FIGURE 5.1: Frequency and amplitude estimation using NLAE (Simulation)

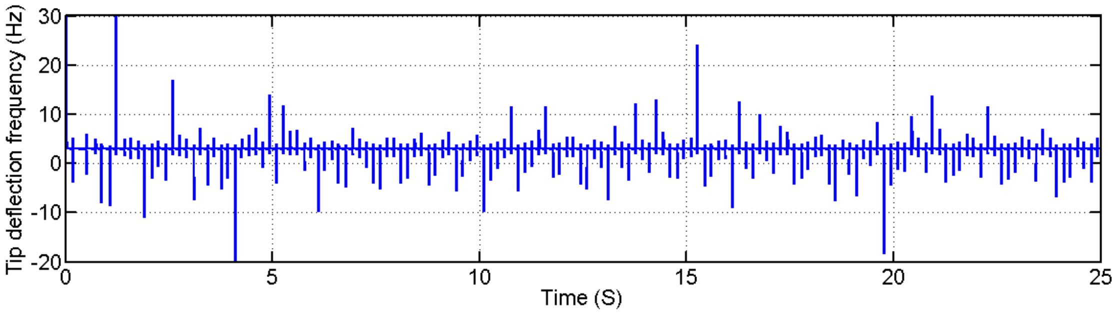

FIGURE 5.2: Frequency and amplitude estimation using AI (Simulation)

The simulation result for the algebraic identification shows the presence of noise of large magnitude and the estimated frequency remains constant with time whereas experimentally, the estimated frequency decays to zero with increasing time. The magnitude of spikes present is very large upto 300 and and amplitude cannot be estimated with this method for the decaying exponential signal. The computation time for the frequency with this method is very small i.e. 0.4 sec. It can work for a wide range of frequency and decaying ratio as can be seen from the table 5.2.

The second order generalised integrator computes the frequency in about 1 s for the simulation. For SOGI, the value of k is 2 which controls the convergence time and γ is -250.

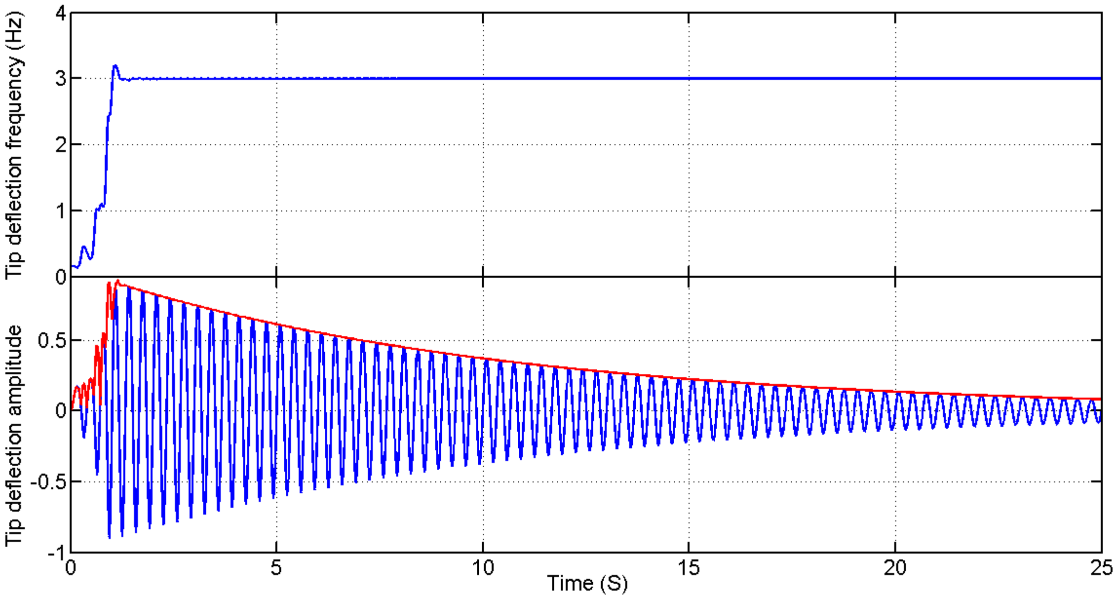

FIGURE 5.3: Frequency and amplitude estimation using SOGI-FLL (Simulation)

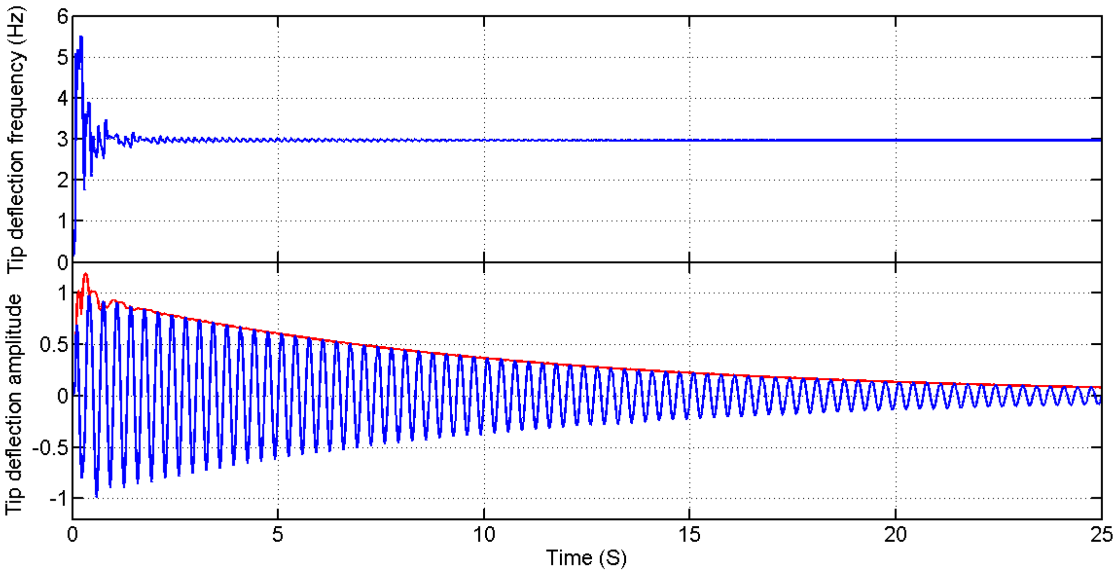

FIGURE 5.4: Frequency and amplitude estimation using TOGI-AFLL (Simulation)

The third order generalised integrator based on adaptive frequency locked loop computes the frequency in about 1 s for both simulation and single-link flexible manipulator. The range of frequency for this method is more compared to SOGI varying from 0.2 to 5.8 but the deacying ratio varies from 0.05 to 0.1 which is less in comparison to other methods. The value of k_s affects the bandwidth of the system and has been set to 2 and γ_s is set to 125.

Fig.5.5 shows the frequency and amplitude estimation with the proposed MWDFT-FLL where the convergence time is 3.5 sec.

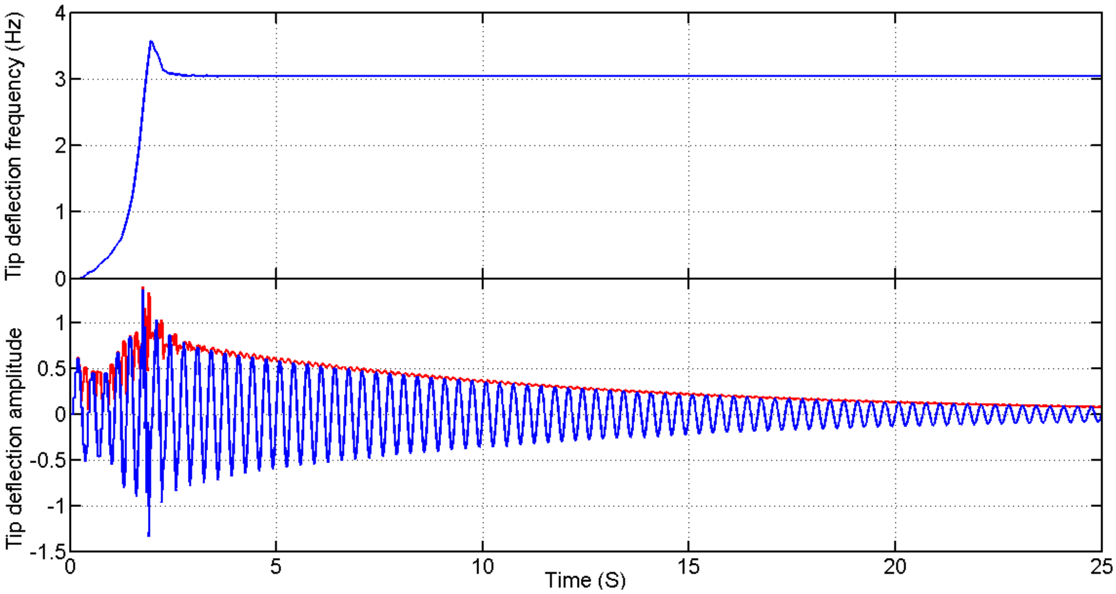

FIGURE 5.5: Frequency and amplitude estimation using MWDFT-FLL (Simulation)

5.1.2 Frequency and amplitude estimation for noisy input signal

The tip deflection signal is corrupted by white Gaussian noise of power of 10 W/MHz. The noisy tip deflection signal, estimated frequencies in presence of noise with other methods, and proposed method are shown in Fig. 5.6 to 5.9

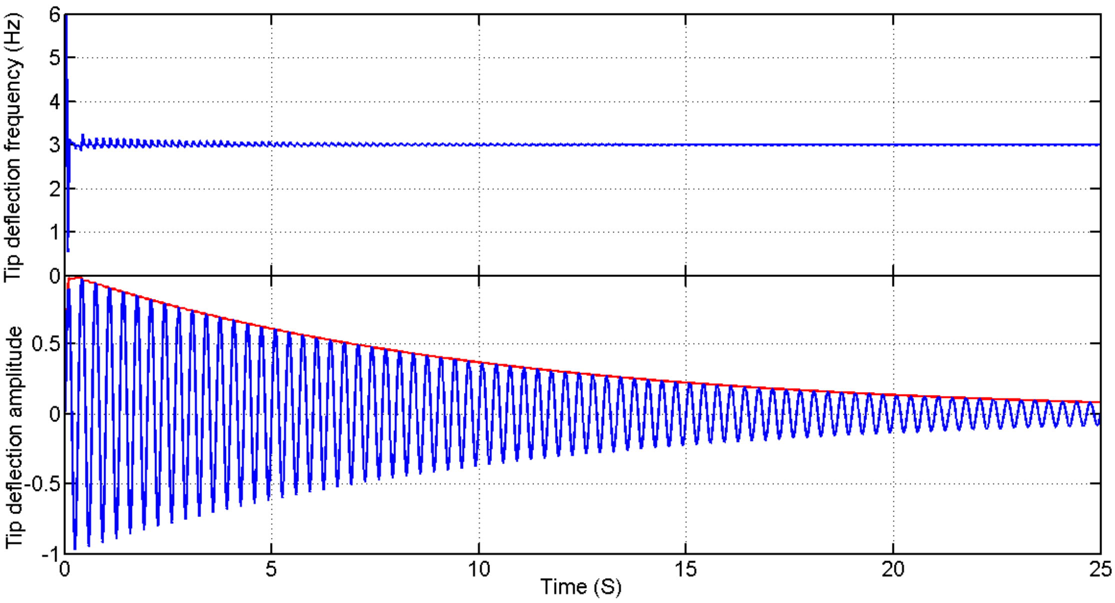

FIGURE 5.6: Frequency and amplitude estimation using NLAE for noisy signal (Simulation)

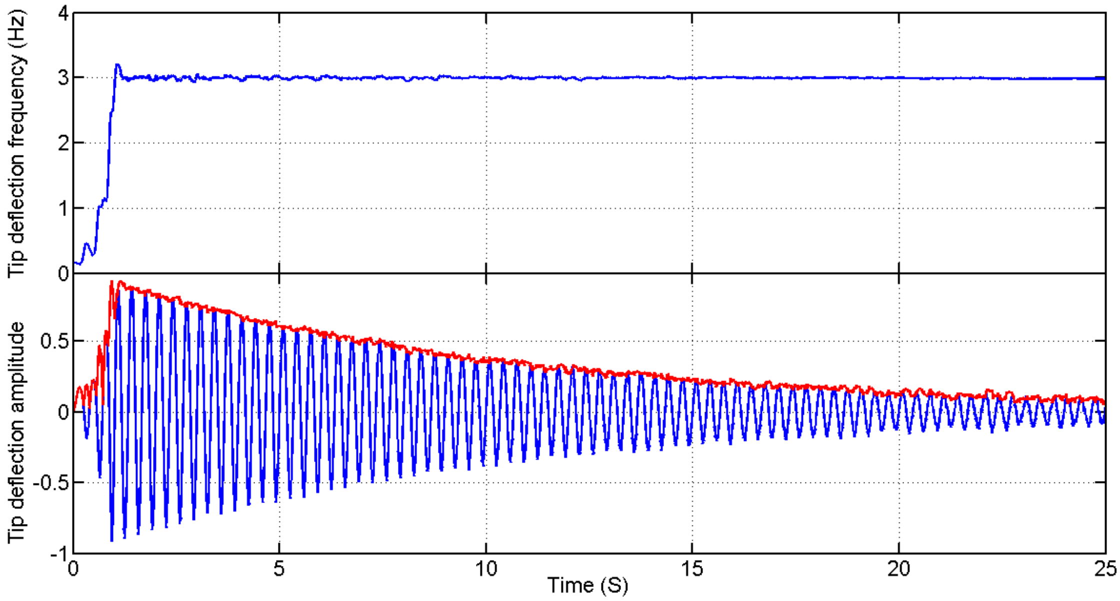

Figure 5.7: Frequency and amplitude estimation using SOGI-FLL for noisy signal (Simulation)

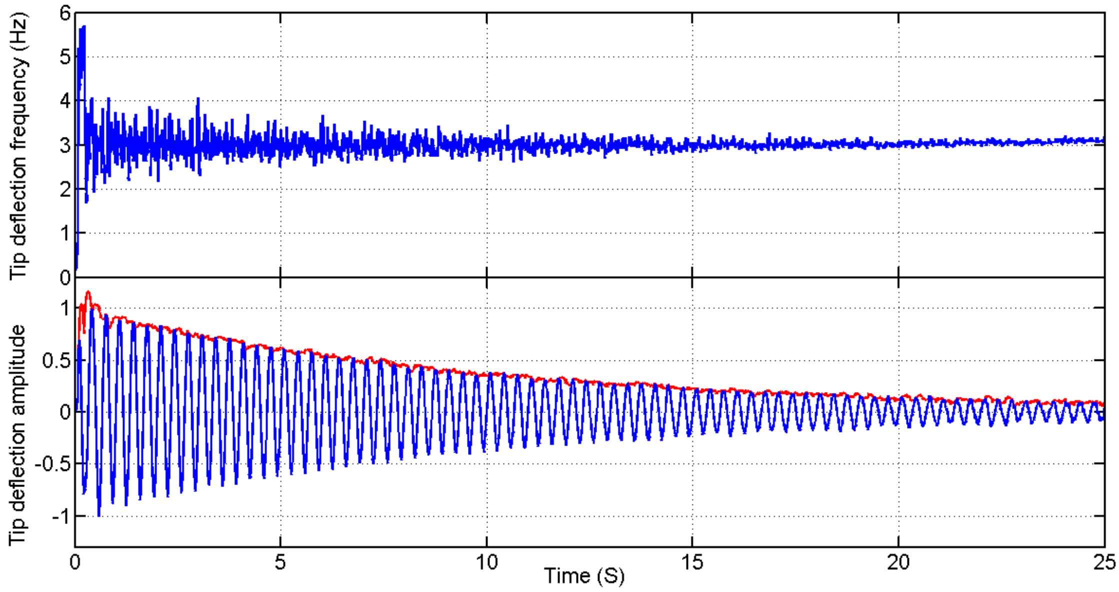

Figure 5.8: Frequency and amplitude estimation using TOGI-AFLL for noisy signal (Simulation)

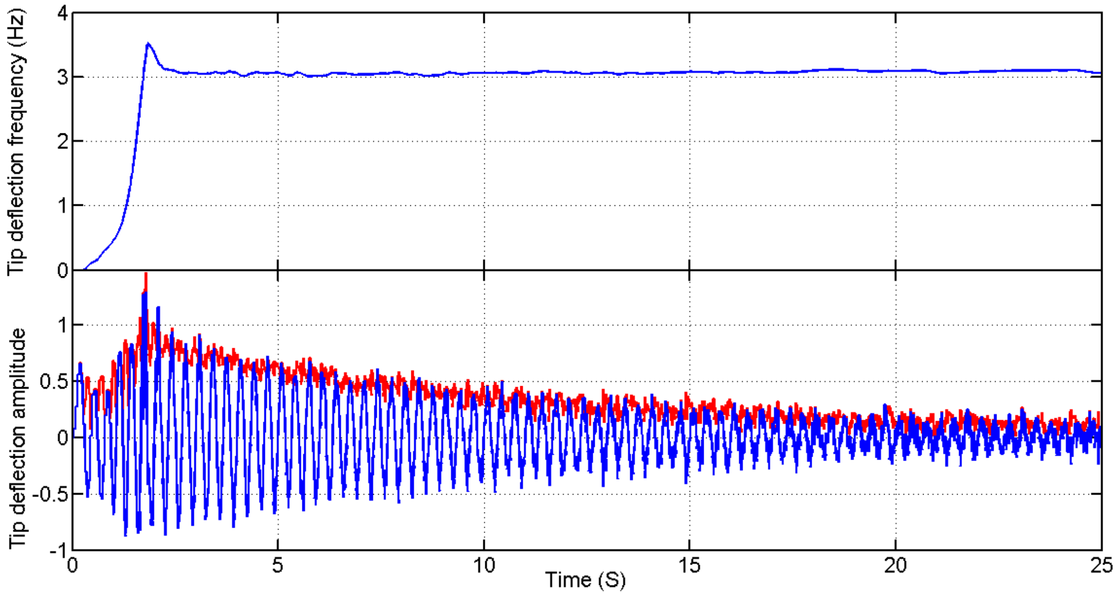

FIGURE 5.9: Frequency and amplitude estimation using MWDFT-FLL for noisy signal (Simulation)

5.1.3 Frequency and amplitude estimation for step changes in amplitude and frequency

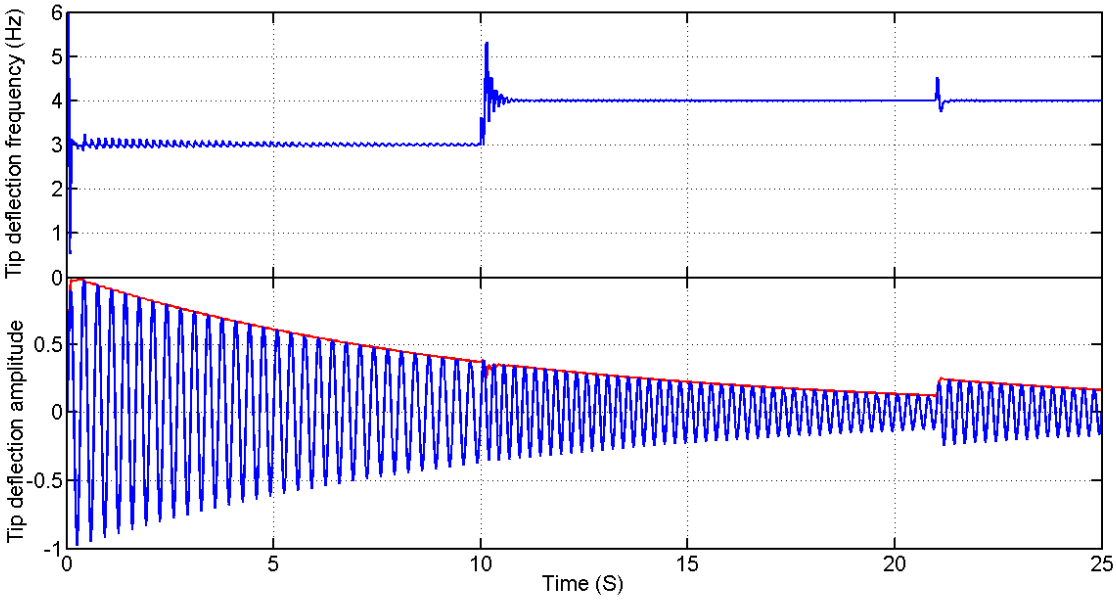

FIGURE 5.10: Frequency and amplitude estimation using NLAE for step changes in frequency and amplitude (Simulation)

The frequency estimations and reconstructed signals with amplitude estimations for the noisy input signal are shown in figures 5.6, 5.7, 5.8 and 5.9. The effect of noise is more in SOGI-FLL and TOGI-AFLL as compared to other methods.

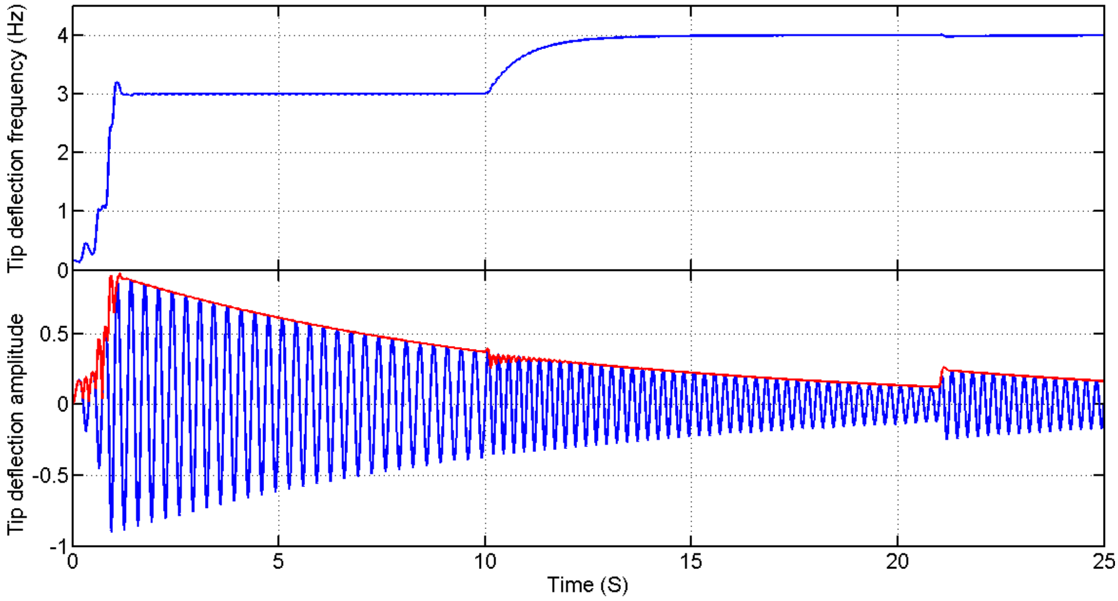

FIGURE 5.11: Frequency and amplitude estimation using SOGI-FLL for step changes in frequency and amplitude (Simulation)

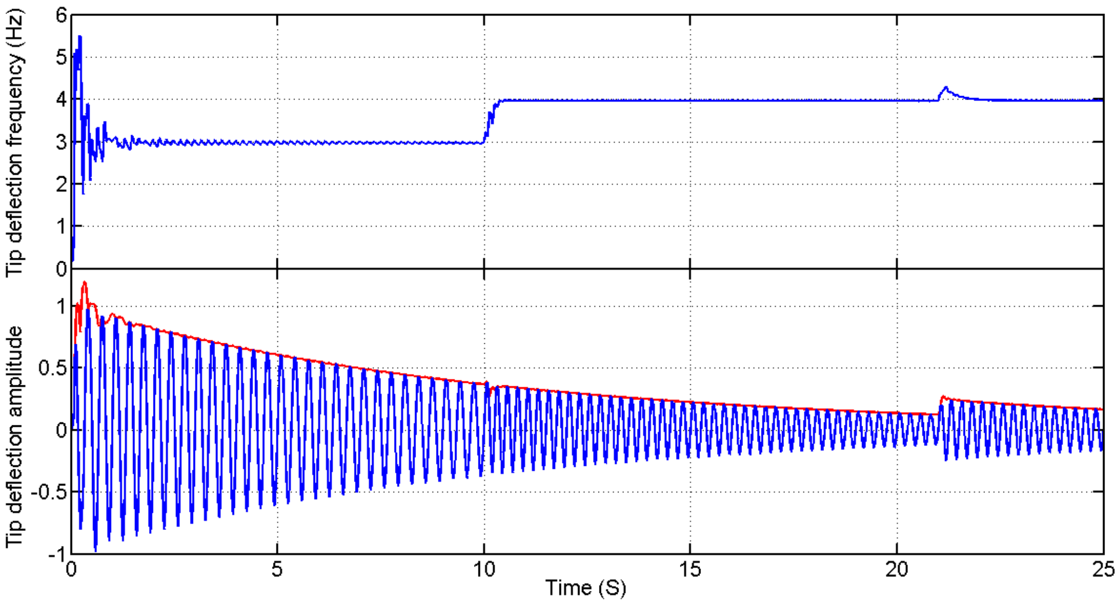

FIGURE 5.12: Frequency and amplitude estimation using TOGI-AFLL for step changes in frequency and amplitude (Simulation)

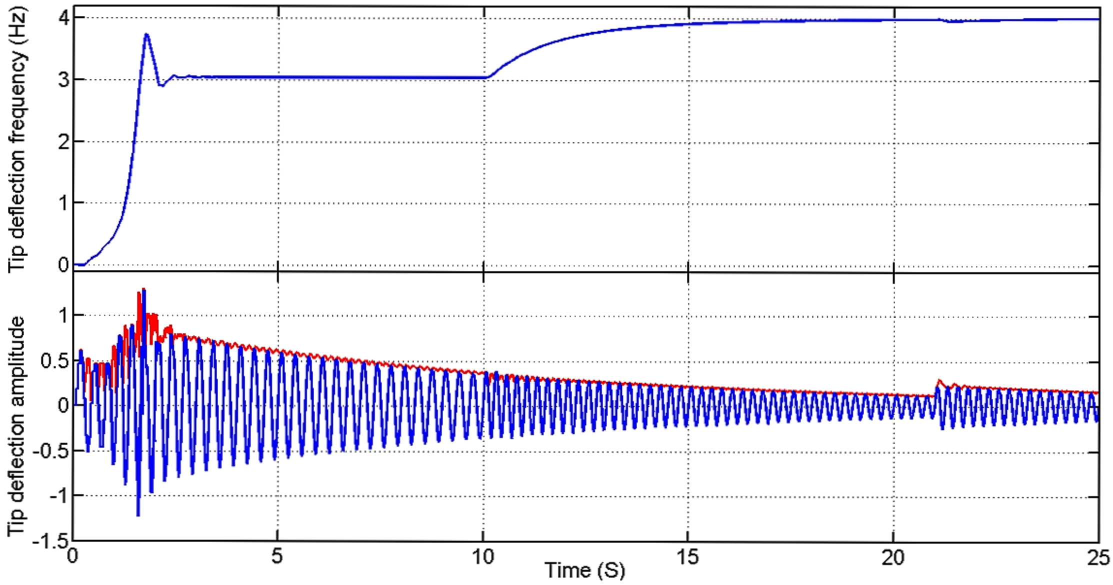

FIGURE 5.13: Frequency and amplitude estimation using MWDFT-FLL for step changes in frequency and amplitude (Simulation)

At 10 s, the step change in frequency of 3 to 3.5 Hz is applied and at 21 s the amplitude of the tip deflection signal is doubled. The estimations of the frequency for the noisy input signal and amplitude estimations with reconstructed signals are shown in figures Fig. 5.10, 5.11, 5.12 and 5.13.

5.1.4 LQR controller

Fig. 5.14 shows the output of LQR controller with full state feedback.

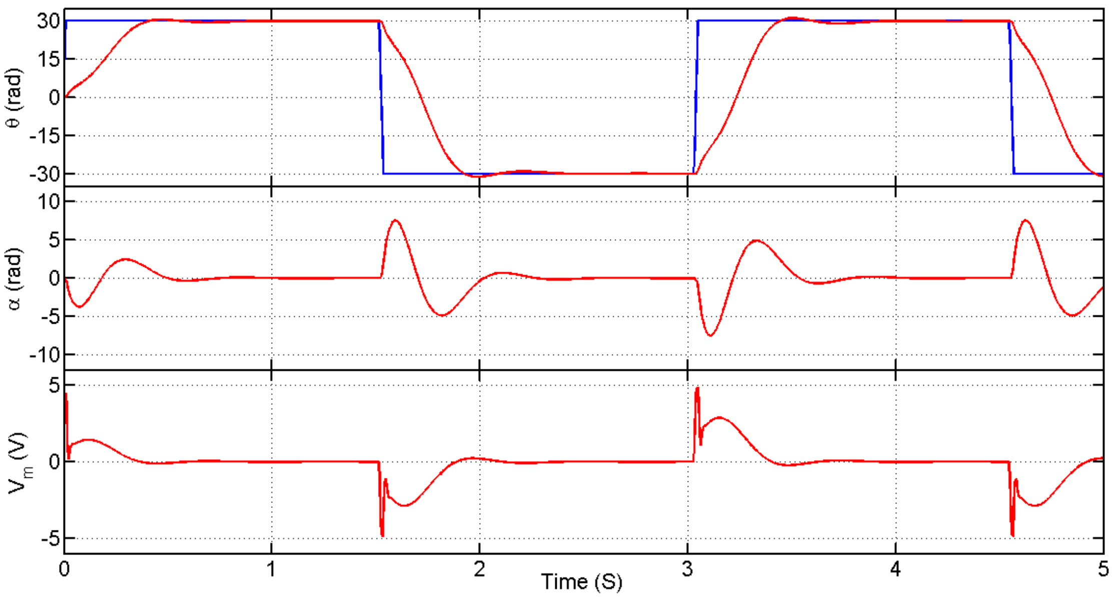

FIGURE 5.14: Output of adaptive controller using LQR - Full state feedback

5.2 Experimental Results

The various methods for frequency estimation as mentioned above have been simulated for a decaying exponential signal and implemented on the experimental set-up. In the experimental setup, the signal from the tip deflection measured by the strain guage is the input to the various techniques. This section discusses the results obtained through experimental validation. The aforementioned methods are tested for determining their operating range for estimating frequency and decaying ratio.

5.2.1 Frequency and amplitude estimation

In GC method, the tuning parameters should be adjusted for estimation of frequency and amplitude every time as frequency or amplitude changes, it was observed that no common set of parameters for particular operating range.

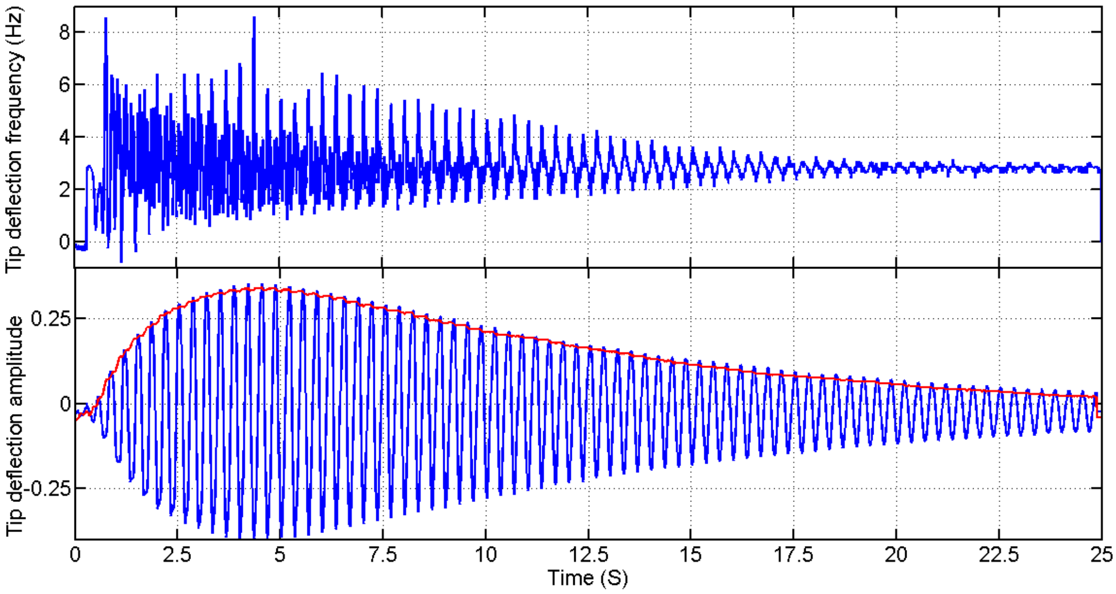

FIGURE 5.15: Frequency and amplitude estimation using NLAE (Experiment)

The measured tip deflection signal with $f = 3\ Hz$, $\zeta = 0.1$, and the estimated frequencies with other methods and MWDFT FLL are shown in Fig. 5.11 to 5.15 respectively. The NLAE provides accurate estimated frequency at steady state, good operating range but the convergence time is 25 s.

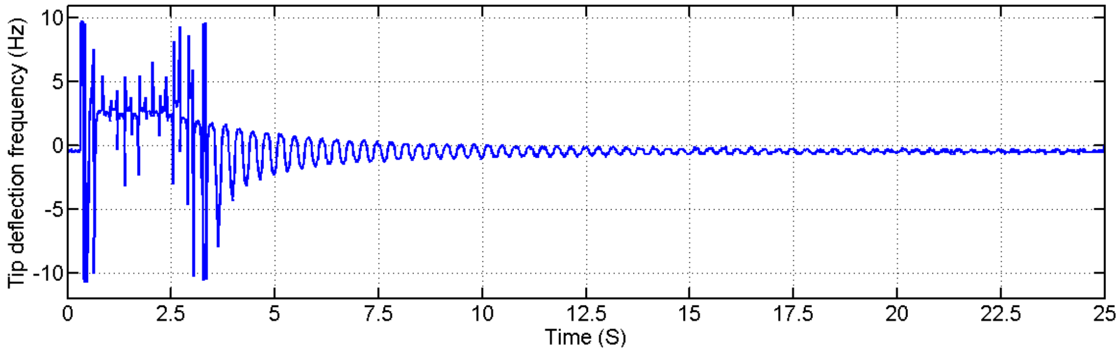

Figure 5.16: Frequency and amplitude estimation using AI (Experiment)

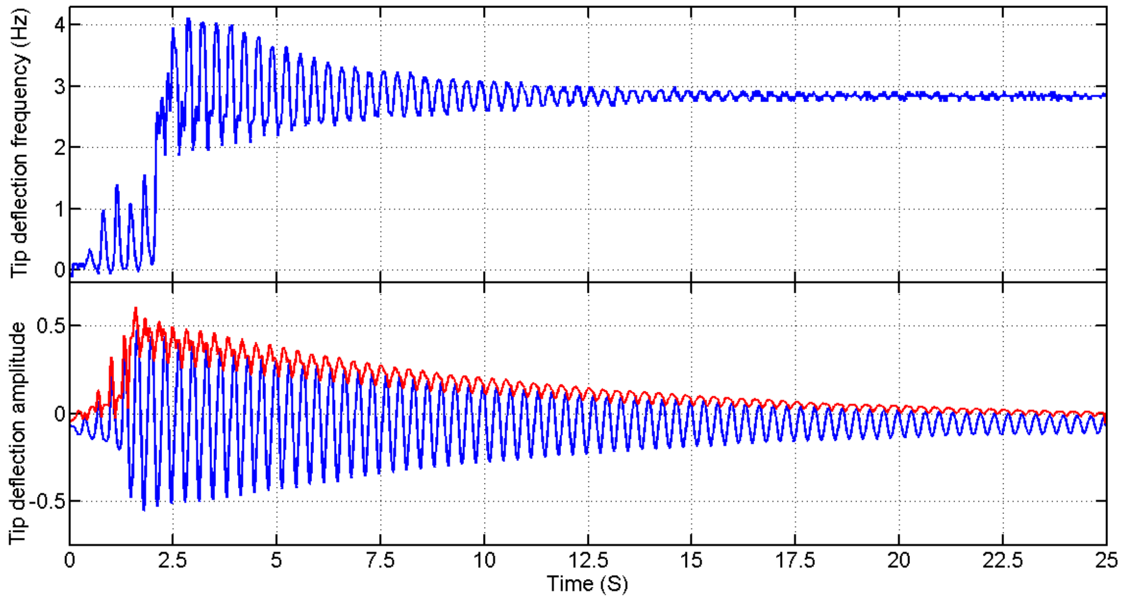

Figure 5.17: Frequency and amplitude estimation using SOGI-FLL (Experiment)

In AI method, 5.16 shows that the estimated frequency decays to zero with increasing time and estimated frequency is noisy. However, AI converges very quickly with 0.4 s. The SOGI FLL exhibits moderate performance for operating range, accuracy and error. However the convergence time is 15 s.

TOGI AFLL also converges at 11 s. The proposed method is tuned to perform for a frequency range of $2.7 - 4.5$ Hz with the decaying ratio range of $0.01 - 1$ for a convergence time of 4 s. The NLAE estimates the amplitude with error whereas the AI method is not suitable for the estimation of amplitude of exponentially decaying sinusoidal signal. The SOGI FLL and TOGI AFLL track the amplitude with oscillations. The proposed method tracks the amplitude accurately. The tip deflection signal and estimated amplitudes with the reconstructed tip deflection signal are shown in Fig. 5.16 to Fig. 5.19.

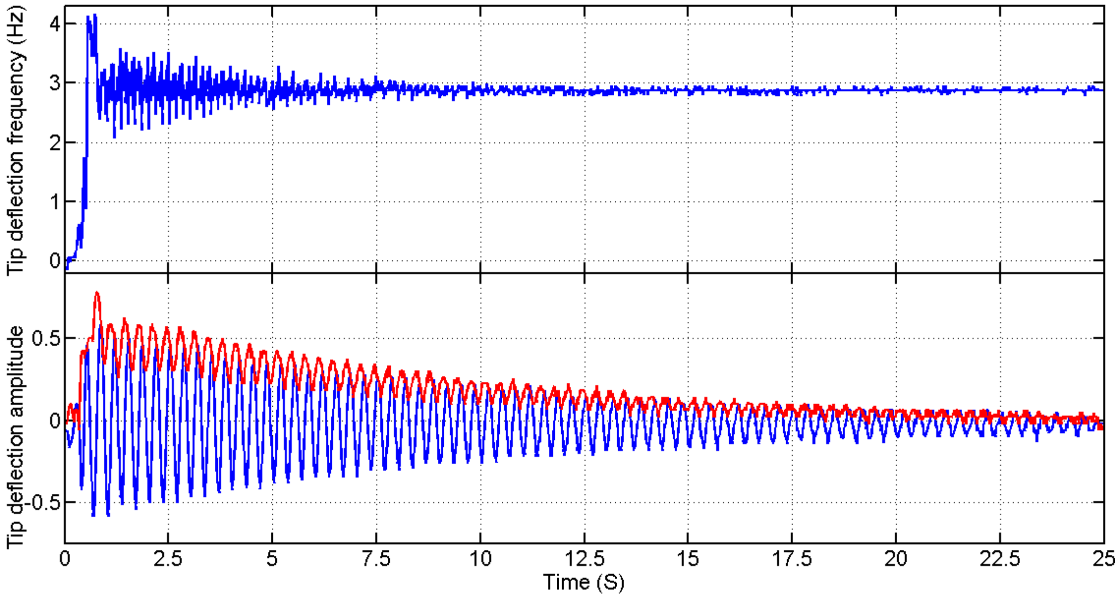

FIGURE 5.18: Frequency and amplitude estimation using TOGI-FLL (Experiment)

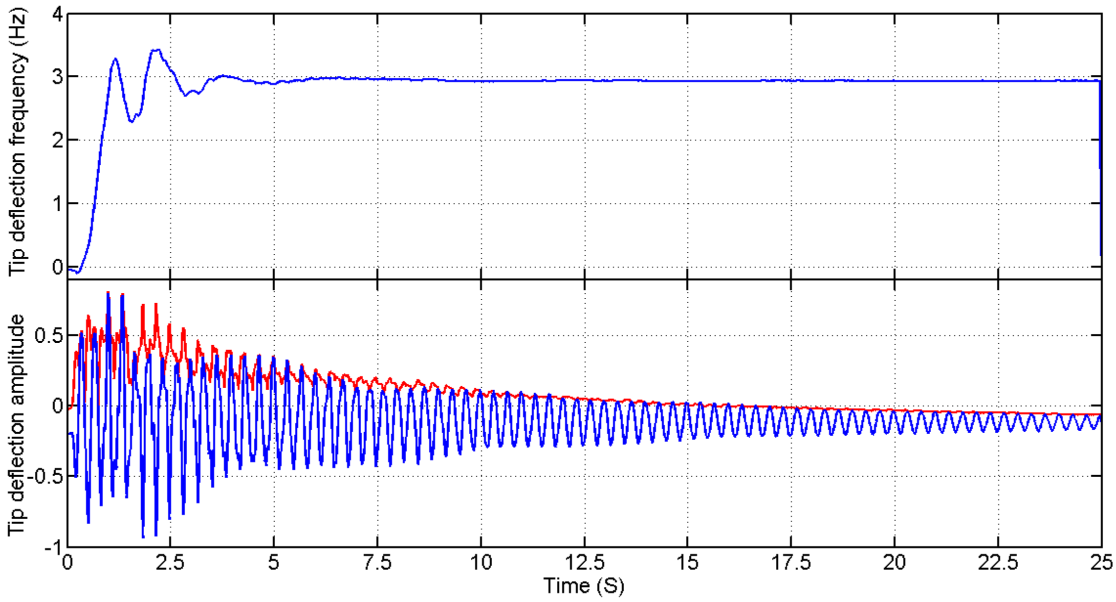

FIGURE 5.19: Frequency and amplitude estimation using MWDFT-FLL (Experiment)

5.2.2 Frequency and amplitude estimation for noisy input signal

The noisy tip deflection signal, estimated frequencies in presence of noise with other methods, and proposed method are shown in Fig. 5.20 to Fig. 5.23 respectively. The tip deflection signal is corrupted by white Gaussian noise of power of 10 W/MHz. The proposed method could track the frequency of the tip deflection signal accurately and it could be observed from the figures. Similarly, the noisy

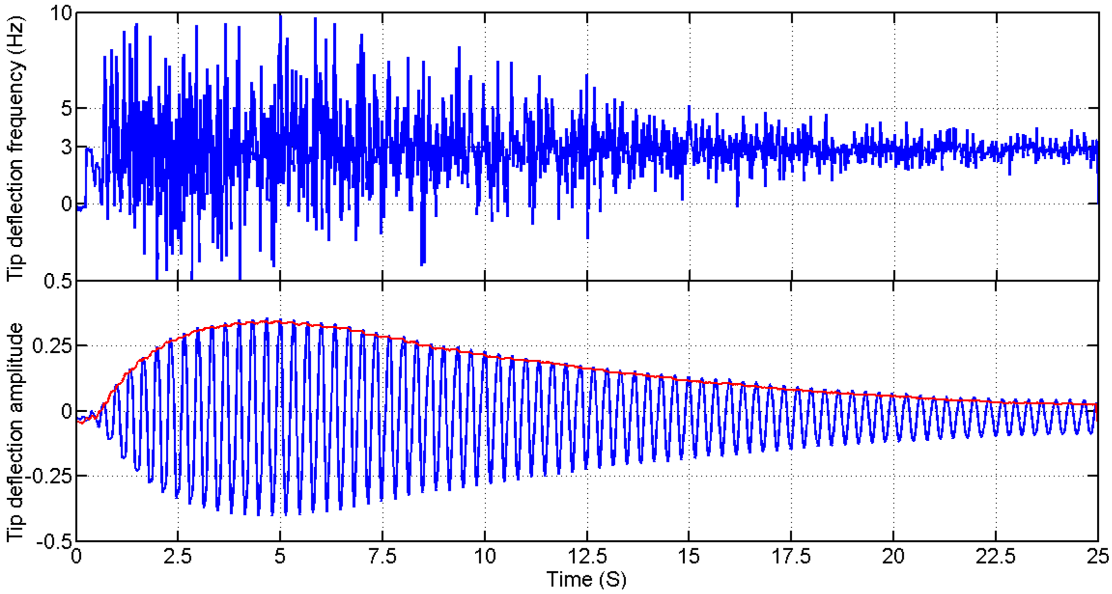

Figure 5.20: Frequency and amplitude estimation using NLAE for noisy signal (Experiment)

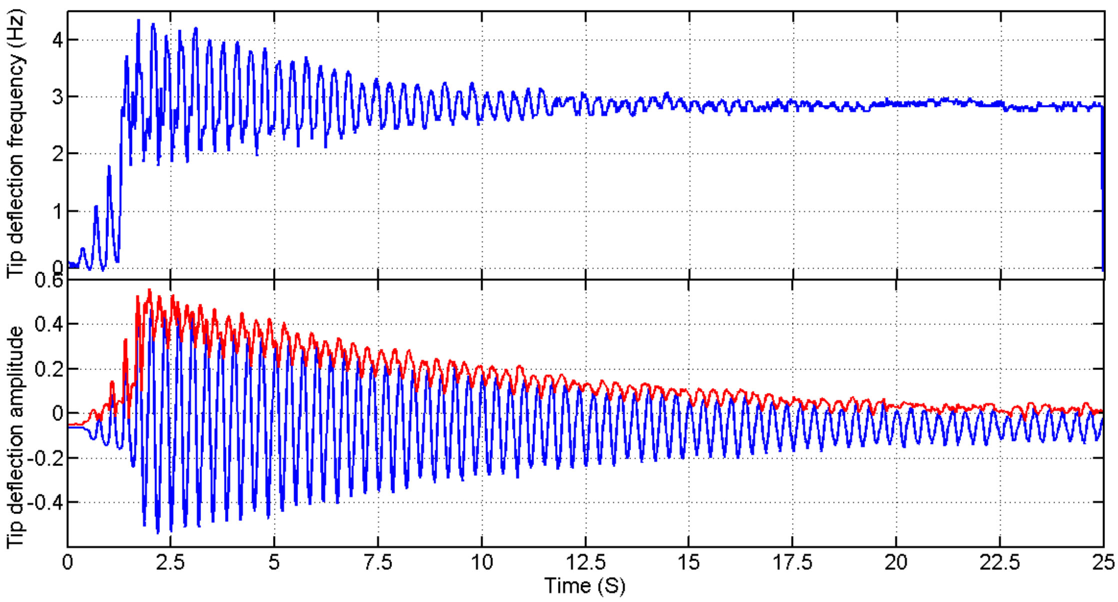

Figure 5.21: Frequency and amplitude estimation using SOGI-FLL for noisy signal (Experiment)

tip deflection signal and the estimated amplitudes with reconstructed signals are shown in Fig. 5.20 to Fig. 5.23 respectively. The proposed method could estimate the amplitude in the presence of noise.

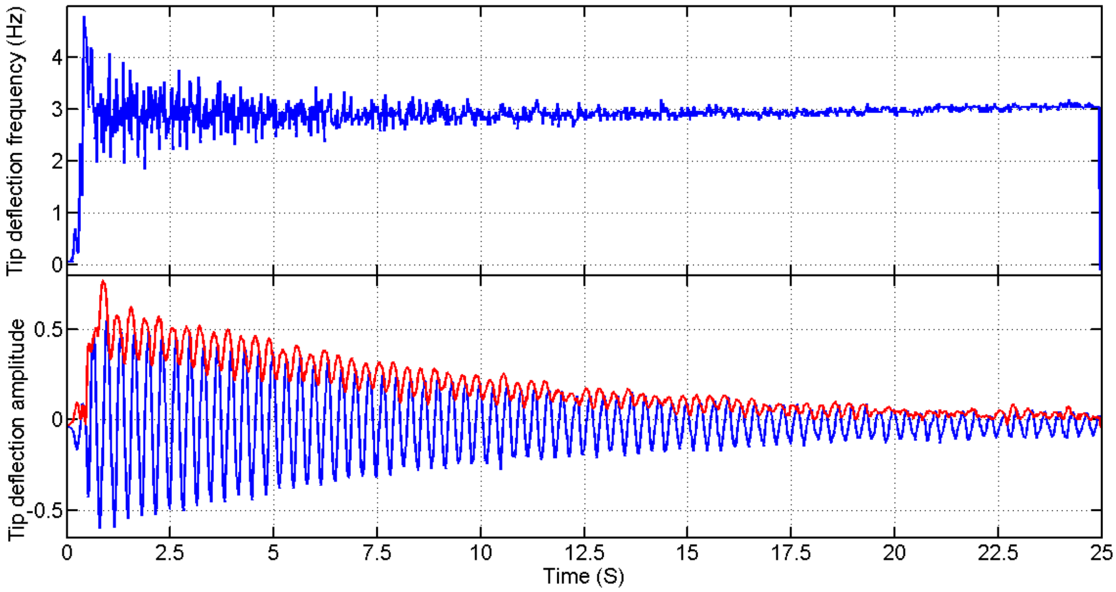

FIGURE 5.22: Frequency and amplitude estimation using TOGI-AFLL for noisy signal (Experiment)

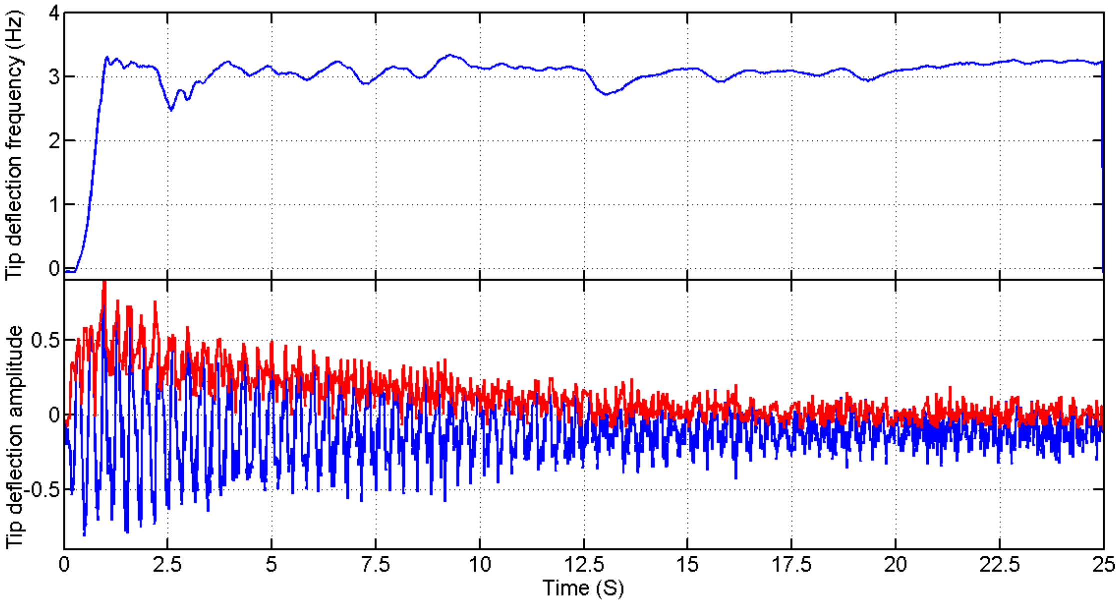

FIGURE 5.23: Frequency and amplitude estimation using MWDFT-FLL for noisy signal (Experiment)

5.2.3 Frequency and amplitude estimation for step changes in amplitude and frequency

The proposed method along with other methods are tested for sudden changes in frequency and amplitude of the tip deflection signal.

At 10 s, the step change in frequency of 3 to 3.5 Hz is applied and at 21 s the amplitude of the tip deflection signal is doubled. The performance of MWDFT

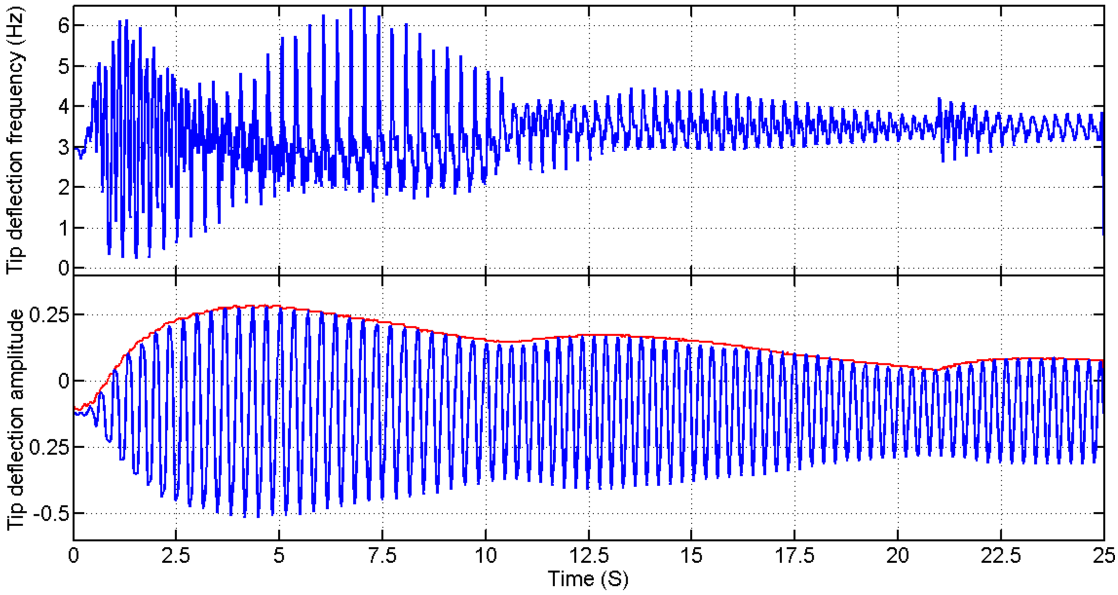

FIGURE 5.24: Frequency and amplitude estimation using NLAE for step changes in frequency and amplitude (Experiment)

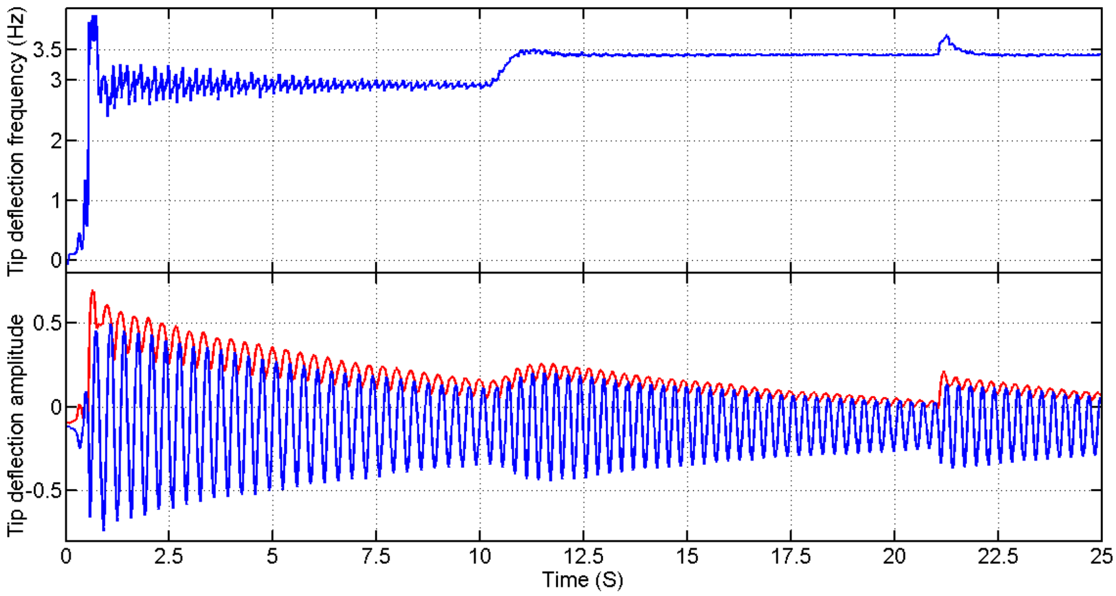

FIGURE 5.25: Frequency and amplitude estimation using SOGI-FLL for step changes in frequency and amplitude (Experiment)

FLL along with other methods are provided in Fig. from 5.24 to 5.27 for frequency estimation. The proposed method converges at 4 s and estimates the frequency accurately. Simultaneously, the amplitude changes are recorded and plotted in Fig. from 5.24 to 5.27 with reconstructed signals.

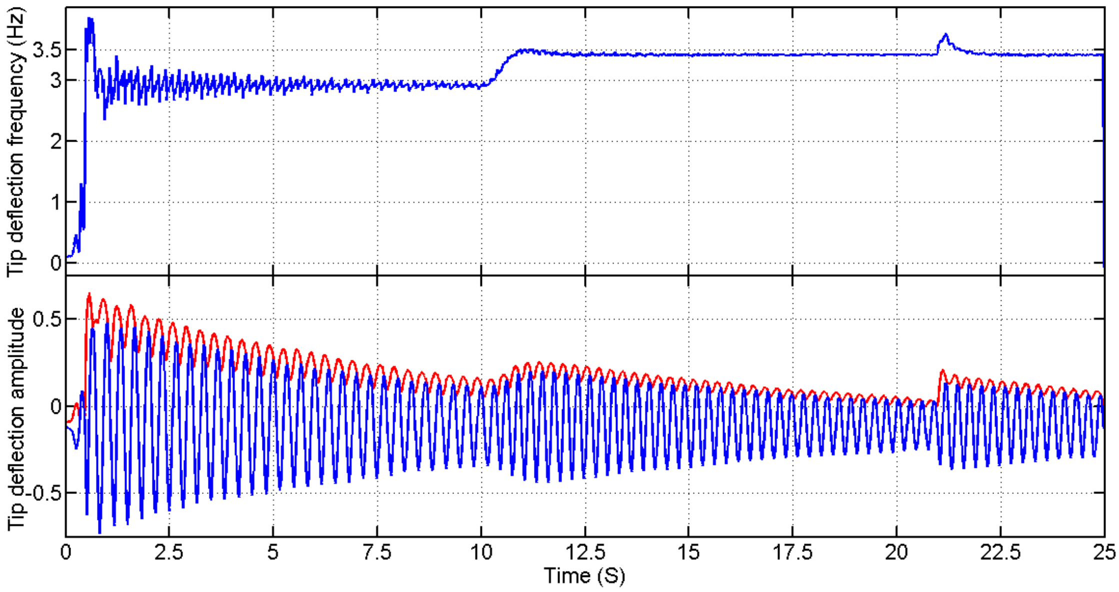

FIGURE 5.26: Frequency and amplitude estimation using TOGI-AFLL for step changes in frequency and amplitude (Experiment)

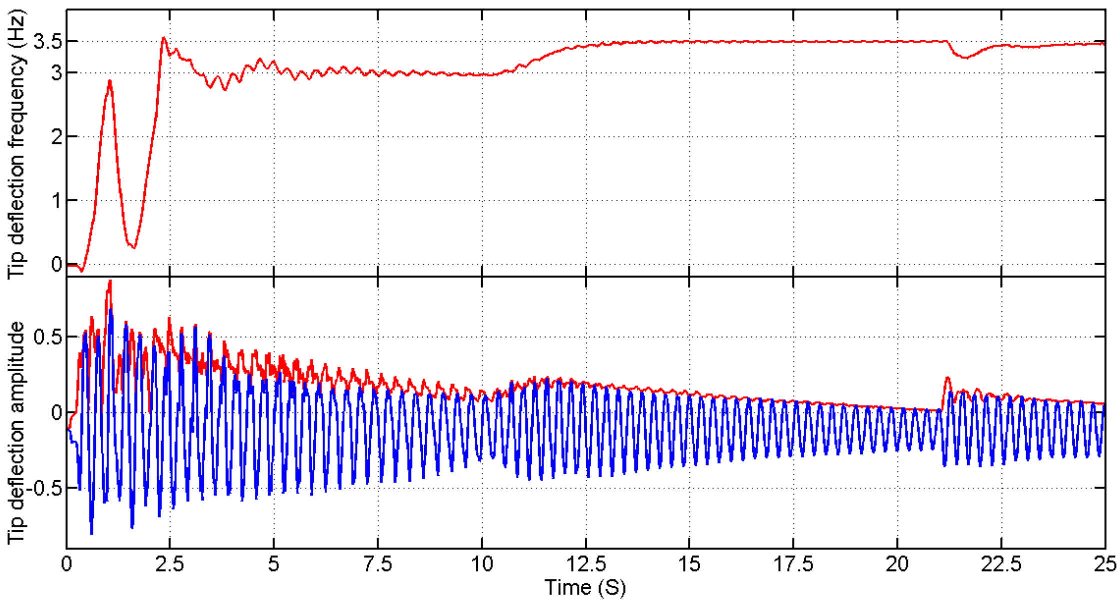

FIGURE 5.27: Frequency and amplitude estimation using MWDFT-FLL for step changes in frequency and amplitude (Experiment)

5.2.4 Performance comparison

It could be observed from 5.29 that the MWDFT FLL performs well in tracking the changes in amplitude.

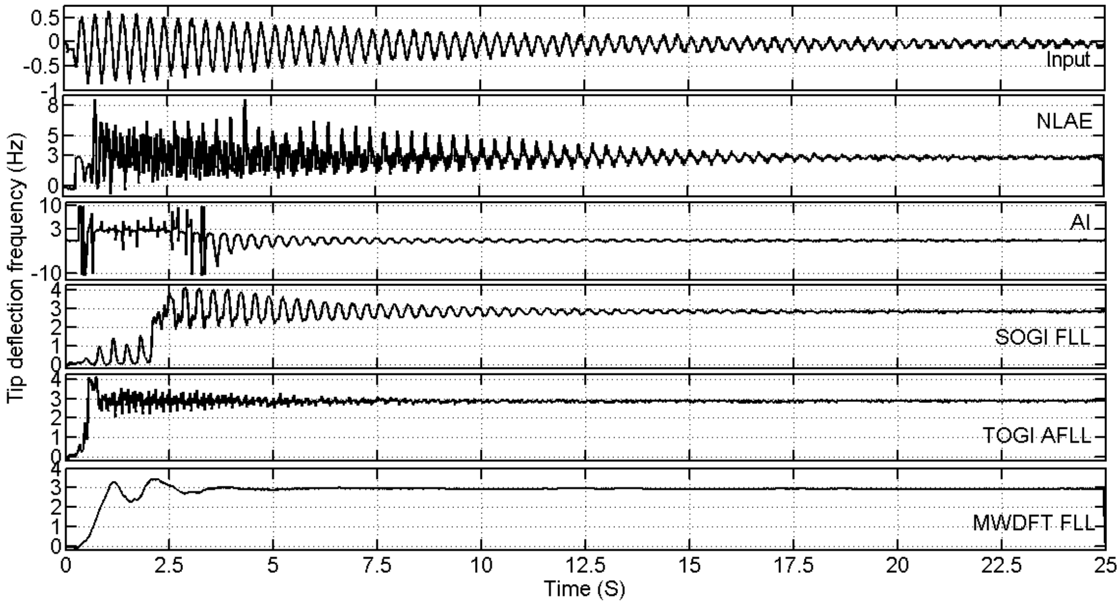

FIGURE 5.28: The tip deflection signal and estimated frequencies (Experiment)

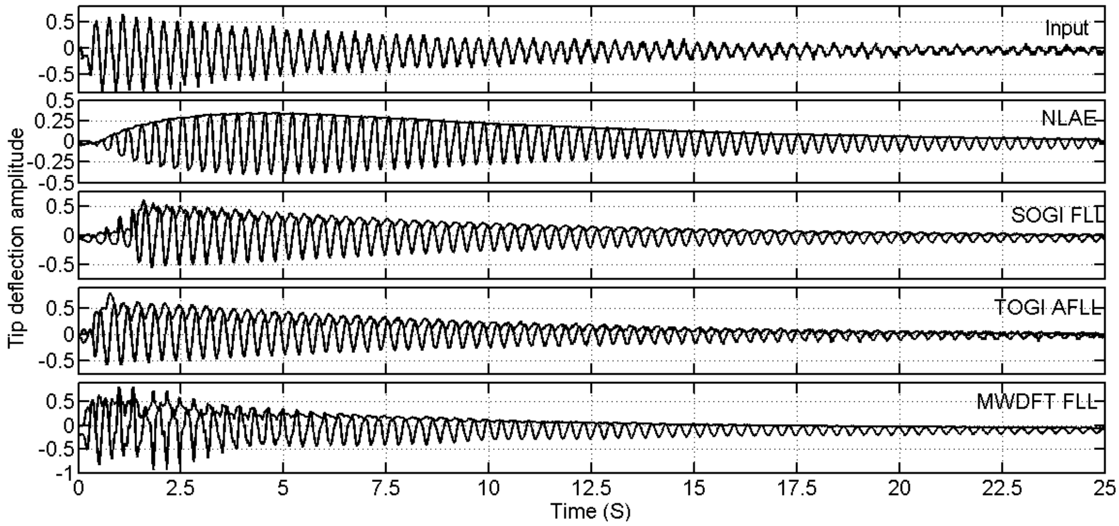

FIGURE 5.29: The tip deflection signal and estimated amplitudes with reconstructed tip deflection signals (Experiment)

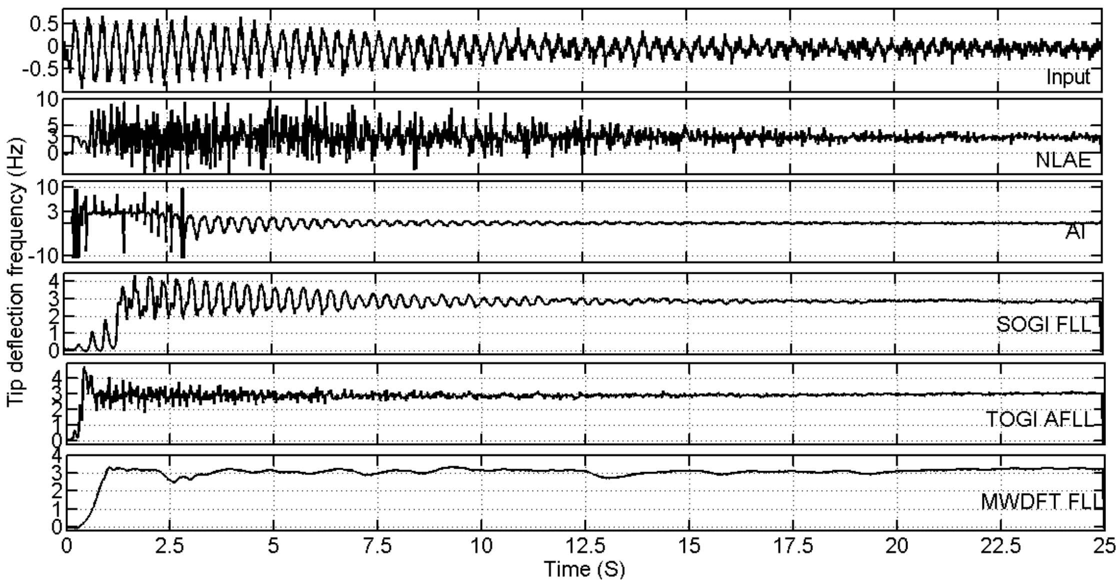

FIGURE 5.30: The noisy tip deflection signal and estimated frequencies (Experiment)

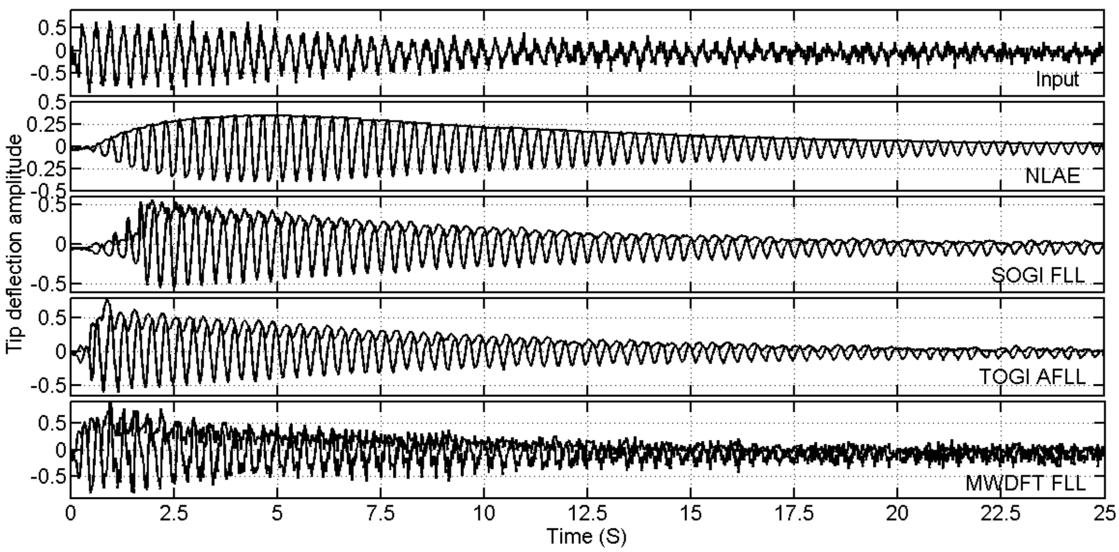

FIGURE 5.31: The noisy tip deflection signal and estimated amplitudes with reconstructed tip deflection signals (Experiment)

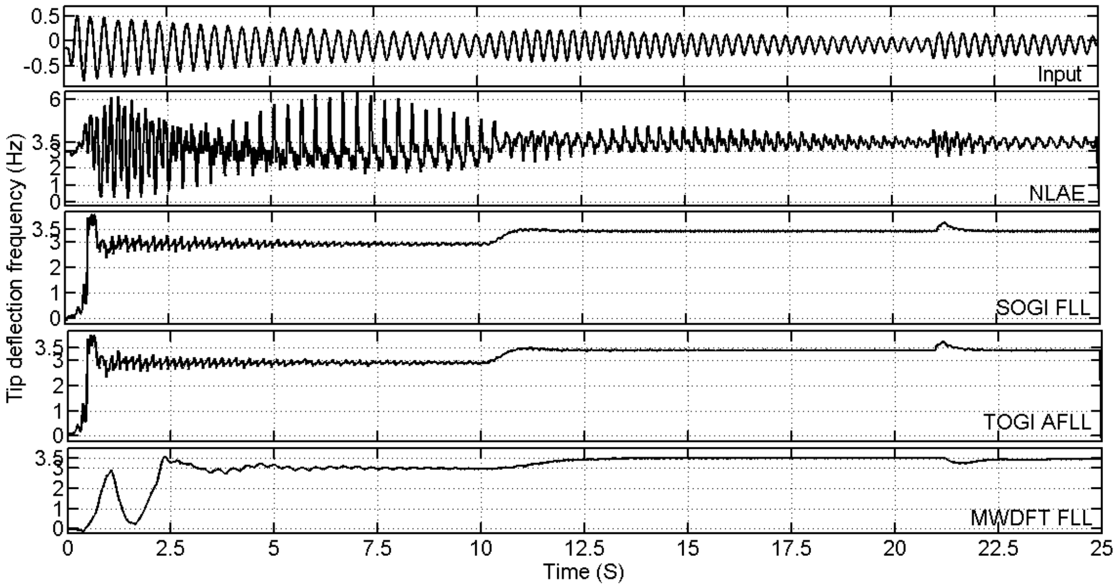

FIGURE 5.32: The tip deflection signal and estimated frequencies for a step change in frequency and amplitude (Experiment)

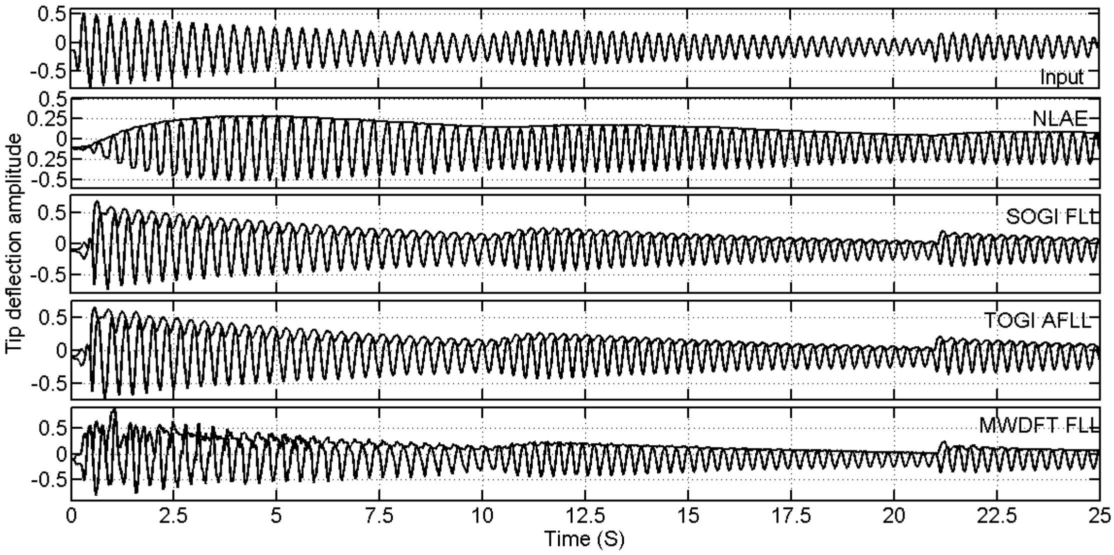

FIGURE 5.33: The tip deflection signal and estimated amplitudes with reconstructed tip deflection signals for a step change in frequency and amplitude (Experiment)

TABLE 5.1: Performance comparison

Parameters	NLAE	GC	AI	SOGI FLL	TOGI AFLL	MWDFT FLL
Range of estimated f (Hz)	1.5 - 6	NA	0.1 - 6	1 - 4.4	0.2 - 5.8	2.7 - 4.5
Range of ζ	0.03 - 1.3	NA	0.01 - 2	0.01 - 0.17	0.01 - 0.8	0.01 - 1
Estimated parameters						
$(f = 3\ Hz;\ \zeta = 0.1)$	NLAE	GC	AI	SOGI FLL	TOGI AFLL	MWDFT FLL
f (Hz)	3.002	NA	NA	2.9	2.975	3.009
Error in f	0.002	NA	NA	0.065	0.025	0.009
Error in amplitude	0.003	NA	NA	0.03	0.013	0.012
Convergence time (s)	25	NA	0.4	15	11	4

TABLE 5.2: Tuning parameters

NLAE	SOGI FLL	TOGI AFLL	MWDFT FLL
$\mu_1 = 1;\ \mu_2 = 0.125;\ \mu_3 = 4000$	$K = 1.3;\ \gamma = -3000$	$K = 2;\ \gamma = 125$	$K = 12;\ K_I = 1.5;\ K_f = 0.9202$

The performance comparison is provided in Table 5.1 and tuning parameters used in the estimation procedure are provided in Table 5.2.

5.2.5 LQR controller

Fig. 5.34 and 5.35 show the output of LQR controller with full state feedback and partial state feedback.

The link deflection α is dampened i.e. oscillations are reduced and the settling time is achieved to be within range. With the partial state feedback controller, only servo angle is controlled and the oscillations are not much dampened. The tuning parameters and attained specifications for the controller are

$q_1 = 125, q_2 = 1, q_3 = 1, q_4 = 5$

$R = 1$

$K = [11.2 \ \ -30.5 \ 1.46 \ \ -0.68]$

$t_s = 0.48s \ \ ; PO = 1.9\% \ ; |\alpha|_{max} = 9.2\,\text{deg}$

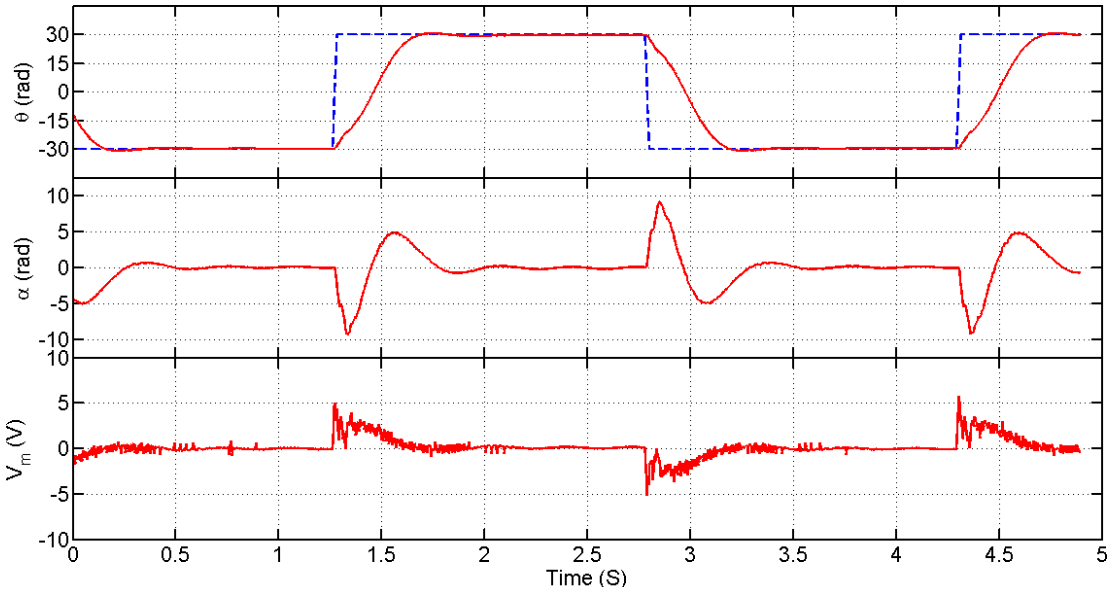

FIGURE 5.34: Output of LQR controller using LQR - full state feedback (Experiment)

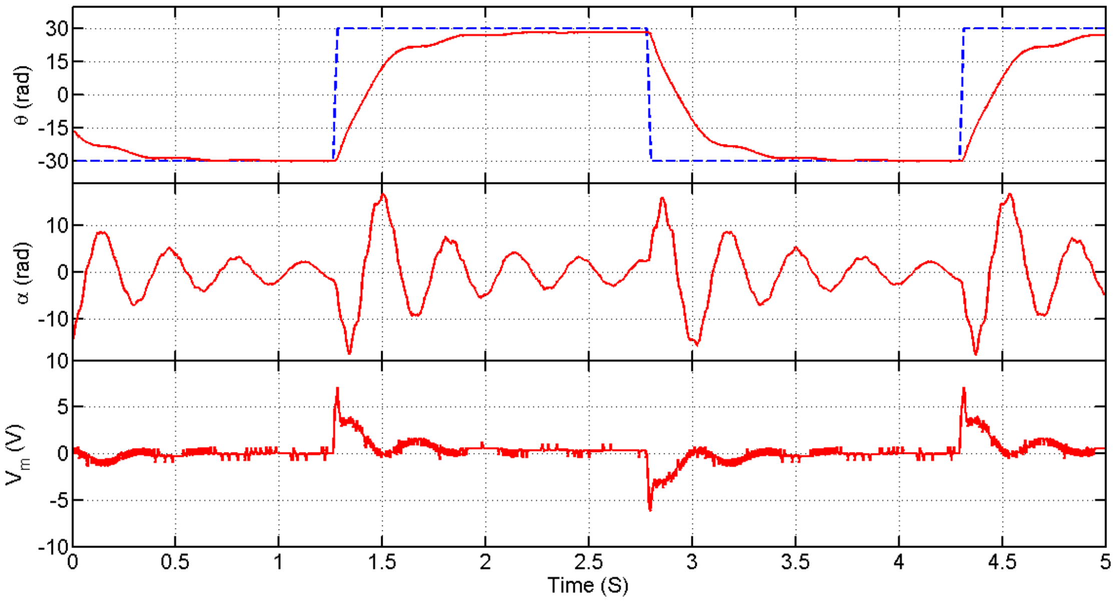

FIGURE 5.35: Output of LQR controller using LQR - partial state feedback (Experiment)

Chapter 6

Conclusion and Future Work

The proposed MWDFT based FLL is experimentally validated as vibration frequency estimator for SLFM. The proposed estimator performs well in estimating the amplitude and frequency of tip deflection signal with good accuracy. In addition, it offers good range for frequency and amplitude estimations with faster decaying ratio. Further, the convergence time for parameter estimation is better compared with SOGI FLL and TOGI AFLL. The proposed method could estimate frequency and amplitude in the presence of noise as well.

It is found that the LQR controller can partially and fully control the servo angle and the flexible link angle thereby effectively suppressing the oscillations.

Adaptive controller can be designed using the proposed technique for frequency estimation.

Publications

1. Shikha Tomar and P. Sumathi, "A Moving-Window DFT based Frequency Locked-Loop for Vibration Frequency Estimation of Single-Link Flexible Manipulator", *IEEE Transactions on Automatic Control* (Under Review).

Bibliography

[1] S. K. Dwivedy and P. Eberhard, “Dynamic analysis of flexible manipulators, a literature review,” *Mech. Mach. Theory,* vol. 41, no. 7, pp. 749-777, Jul. 2006.

[2] S. K. Tso, T. W. Yang, W. L. Xu and Z. Q. Sun, “Vibration Control for a Flexible-Link Robot Arm with Deflection Feedback,” *Int. J. Non-Linear Mech.,* vol. 38, no. 1, pp. 51-62, Jan. 2003.

[3] H. Geniele, R. V. Patel and K. Khorasani, “End-point Control of a Flexible-Link Manipulator: Theory and Experiments,” *IEEE Trans. Control Syst. Technol.,* vol. 5, no. 6, pp. 556-570, Nov. 1997.

[4] C. A. Monje, F. Ramos, V. Feliu and B. M. Vinagre, “Tip Position Control of a Lightweight Flexible Manipulator using a Fractional Order Controller,” *IET Control Theory Appl.,* vol. 1, no. 5, pp. 1451-1460, Sep. 2007.

[5] J. Becedas, I. Payo and V. Feliu, “Generalised proportional integral torque control for single-link flexible manipulators,” *IET Control Theory Appl.,* vol. 4, no. 5, pp. 773-783, May 2010.

[6] Z. Su and K. Khorasani, “A neural-network-based controller for a single-link flexible manipulator using the inverse dynamics approach,” *IEEE Trans. Industrial Electronics,* vol. 48, no. 6, pp. 1074-1086, Dec. 2001.

[7] F. M. Caswara and H. Unbehauen, “A neurofuzzy approach to the control of a flexible-link manipulator,” *IEEE Trans. Robot. Autom.,* vol. 18, no. 6, pp. 932-944, Dec. 2002.

[8] A. Jnifenea and W. Andrews, “Experimental study on active vibration control of a single-link flexible manipulator using tools of fuzzy logic and neural networks,” *IEEE Trans. Instrumentation and Measurement,* vol. 54, no. 3, pp. 1200-1208, Jun 2015.

[9] E. Pereira, S. S. Aphale, V. Feliu and S. O. R. Moheimani, “Integral Resonant Control for Vibration Damping and Precise Tip-Positioning of a Single-Link Flexible Manipulator,” *IEEE/ASME Trans. Mechatronics,* vol. 16, no.2, pp. 232-240, Apr. 2011.

[10] M. R. Rokui and K. Khorasani, “Experimental results on discrete-time nonlinear adaptive tracking control of a flexible-link manipulator,” *IEEE Trans. Syst. Man Cybern. B, Cybern.,* vol. 30, no. 1, pp. 151-164, Feb. 2000.

[11] T.-C. Yang, J. C. S. Yang and P. Kudva, “Adaptive control of a single-link flexible manipulator with unknown load,” *IEE Proc.-D,* vol. 138, no. 2, pp. 153-159, Mar. 1991.

[12] T.-C. Yang, J. C. S. Yang, and P. Kudva, “Load-adaptive control of a single-link flexible manipulator,” *IEEE Trans. Syst. Man Cybern.,* vol. 22, no. 1, pp. 85-91, Jan/Feb. 1992.

[13] G. L.Wang and Y. F. Li, “Integrated sensing and filter design for a singlelink flexible manipulator,” *IEEE Trans. Robot. Autom.,* vol. 20, no. 3, pp. 559-564, Jun. 2004.

[14] V. Feliu and F. Ramos, “Strain gauge based control of single-link flexible very light weight robots robust to payload changes,” *Mechatronics,* vol. 15, no. 5, pp. 547-571, Jun. 2005.

[15] C. Shitole and P. Sumathi, “Sliding DFT-Based Vibration Mode Estimator for Single-Link Flexible Manipulator,” *IEEE/AMSE Trans. Mechatronics,* vol. 20, no. 6, pp. 3249-3256, Dec. 2015.

[16] J. Becedas, J. R. Trapero, V. Feliu, and H. Sira-Ramirez, “Adaptive controller for single-link flexible manipulators based on algebraic identification and generalized proportional integral control,” *IEEE Trans. Syst. Man Cybern. B, Cybern.,* vol. 39, no. 3, pp. 735-751, Jun. 2009.

[17] A. K. Ziarani and A. Konrad, "A Method of Extraction of Nonstationary Sinusoids," *Signal Processing,* vol. 84, no. 8, pp. 1323-1346, Apr. 2004.

[18] M. Hou, "Amplitude and Frequency Estimator of a Sinusoid," *IEEE Trans. Automatic Control,* vol. 50, no. 6, pp. 855-858, Jun. 2005.

[19] L. Hsu, R. Ortega, G. Damm, "A Globally Convergent Frequency Estimator," *IEEE Trans. Automatic Control,* vol. 44, no. 4, pp. 698-713, Apr. 1999.

[20] J. R. Trapero, H. Sira-Ramirez, and V. F. Batlle, "An Algebraic Frequency Estimator for a Biased and Noisy Sinusoidal Signal," *Signal Processing,* vol. 87, no. 6, pp. 1188-1201, Jun. 2007.

[21] J. R. Trapero, H. Sira-Ramirez, and V. F. Batlle, "A Fast On-Line Frequency Estimator of Lightly Damped Vibrations in Flexible Structures," *Journal of Sound and Vibration,* vol. 307, no. 1/2, pp. 365-378, Oct. 2007.

[22] G. Fedele and A. Ferrise, "Non Adaptive Second-Order Generalized Integrator for Identification of a Biased Sinusoidal Signal," *IEEE Trans. Automatic Control,* vol. 57, no. 7, pp. 1838-1842, Jun 2012.

[23] P. Rodriguez, A. Luna, I. Candela, R. Mujal, R. Teodorescu, and F. Blaabjerg, "Multiresonant Frequency-Locked Loop for Grid Synchronization of Power Converters under Distorted Grid Conditions," *IEEE Trans. Ind. Electron.,* vol. 58, no. 1, pp. 127-138, Jan. 2011.

[24] X. Yuan, W. Merk, H. Stemmler, and J. Allmeling, "Stationary-Frame Generalized Integrators for Current Control of Active Power Filters With Zero Steady-State Error for Current Harmonics of Concern Under Unbalanced and Distorted Operating Conditions," *IEEE Trans. Industry Applications,* vol. 38, no. 2, pp. 523-532, Mar./Apr. 2002.

[25] G. Fedele and A. Ferrise, "A Frequency-Locked-Loop Filter for Biased Multi-Sinusoidal Estimation," *IEEE Trans. Signal Process.,* vol. 62, no. 5, pp. 1125-1134, Mar. 2014.

[26] E. Jacobsen, R. Lyons, "The Sliding DFT," *IEEE Signal Processing Magazine,* vol. 20, no. 2, pp. 74-80, Mar. 2003.

[27] E. Jacobsen, R. Lyons, “An Update to the Sliding DFT,” *IEEE Signal Processing Magazine,* vol. 21, no.1, pp. 110-111, Jan. 2004.

[28] J. A. Rosendo Macias and A. Gomez Exposito, “Efficient Moving-Window DFT Algorithms,” *IEEE Trans. Circuits and Systems-II: Analog and Digital Signal Processing,* vol. 45, no.2, pp. 256-260, Feb. 1998.

[29] C.S. Turner, “Recursive Discrete-Time Sinusoidal Oscillators,” *IEEE Signal Processing Magazine,* vol. 20, no.3, pp. 103-111, May 2003.